HHS Public Access

Author manuscript

Oncogene. Author manuscript; available in PMC 2024 December 10.

Published in final edited form as:

Oncogene. 2024 July ; 43(31): 2431–2446. doi:10.1038/s41388-024-03078-1.

Estrogen-related receptor alpha promotes thyroid tumor cell survival via a tumor subtype-specific regulation of target gene networks

Wenjing Chen[*,1], **Young Shin Song**[*,2,3], **Han Sai Lee**[2,3], **Chien-Wei Lin**[4], **Junguee Lee**[5], **Yea Eun Kang**[6], **Seon-Kyu Kim**[7], **Seon-Young Kim**[8], **Young Joo Park**[3,9], **Jong-In Park**[1]

[1]Department of Biochemistry, Medical College of Wisconsin, Milwaukee, WI 53226, USA

[2]Department of Internal Medicine, Seoul Metropolitan Government Seoul National University Boramae Medical Center, Seoul, Republic of Korea

[3]Department of Internal Medicine, Seoul National University College of Medicine, Seoul, Republic of Korea

[4]Division of Biostatistics, Institute for Health and Equity, Medical College of Wisconsin, Milwaukee, WI 53226, USA

[5]Department of Pathology, Konyang University School of Medicine, Daejeon, Republic of Korea

[6]Division of Endocrinology and Metabolism, Department of Internal Medicine, Chungnam National University Hospital & College of Medicine, Daejeon, Republic of Korea.

[7]Personalized Genomic Medicine Research Center, Korea Research Institute of Bioscience and Biotechnology, Daejeon, Republic of Korea

[8]Korea Bioinformation Center, Korea Research Institute of Bioscience and Biotechnology, Daejeon, Republic of Korea

[9]Department of Molecular Medicine and Biopharmaceutical Sciences, Graduate School of Convergence Science and Technology, Seoul National University, Seoul, Republic of Korea

Abstract

Mortalin (encoded by *HSPA9*) is a mitochondrial chaperone often overexpressed in cancer through as-yet-unknown mechanisms. By searching different RNA-sequencing datasets, we found that *ESRRA* is a transcription factor highly correlated with *HSPA9* in thyroid cancer, especially in follicular, but not C cell-originated, tumors. Consistent with this correlation, ESRRA depletion decreased mortalin expression only in follicular thyroid tumor cells. Further, ESRRA expression

Corresponding author: Jong-In Park, jipark@mcw.edu.

*These two authors contributed equally to this work

Author contributions

Conceptualization, WC and JIP; methodology, WC, YSS, HSL, CWL, JL and JIP; formal analysis, WC, YSS, HSL, CWL, JL, YEK, SKK, SYK, and JIP; investigation, WC, YSS, HSL, CWL, JL and JIP; validation, WC, YSS, HSL and JIP; writing—original draft preparation, WC, YSS, and JIP; writing-review and editing, WC, YSS, YJP and JIP; visualization, WC, YSS, HSL, CWL, JL and JIP; supervision, YJP and JIP; project administration, JIP; funding acquisition, JIP. All authors have read and agreed to the published version of the manuscript.

Conflict of interest: The authors have no conflict of interest to declare

and activity were relatively high in thyroid tumors with oncocytic characteristics, wherein ESRRA and mortalin exhibited relatively high functional overlap. Mechanistically, ESRRA directly regulated *HSPA9* transcription through a novel ESRRA-responsive element located upstream of the *HSPA9* promoter. Physiologically, ESRRA depletion suppressed thyroid tumor cell survival via caspase-dependent apoptosis, which ectopic mortalin expression substantially abrogated. ESRRA depletion also effectively suppressed tumor growth and mortalin expression in the xenografts of oncocytic or ESRRA-overexpressing human thyroid tumor cells in mice. Notably, our Bioinformatics analyses of patient data revealed two ESRRA target gene clusters that contrast oncocytic-like and anaplastic features of follicular thyroid tumors. These findings suggest that ESRRA is a tumor-specific regulator of mortalin expression, the ESRRA-mortalin axis has higher significance in tumors with oncocytic characteristics, and ESRRA target gene networks can refine molecular classification of thyroid cancer.

Keywords

Thyroid cancer; tumor subtype; ESRRA; mortalin/HSPA9; transcription

Introduction

Thyroid cancer is the most common neoplasm of the endocrine system and the seventh most frequent human malignancy among females in the United States, with rapidly rising incidence [1]. Thyroid cancer is histologically classified as follicular- and C-cell-originated tumors [2]. Follicular cell-originated tumors include papillary thyroid carcinoma (PTC, over 70% of all thyroid carcinomas), follicular thyroid carcinoma (FTC, 10–20%), anaplastic thyroid carcinoma (ATC, 1–2%), and oncocytic carcinomas of the thyroid (OCA, 3–5%), while C cell-originated tumors present exclusively medullary thyroid carcinoma (MTC, 3–5%). PTC and FTC generally show favorable prognoses with nearly 100% 5-year survival [1]. OCA is relatively aggressive, with a 5-year survival of 65–91% [3–5]. ATC is the most aggressive type, with only 7% 5-year survival [6]. Metastatic aggressive MTC also shows an unfavorable prognosis of about 89% 5-year survival [1]. Despite decades of pathophysiological mechanism studies, therapeutic modality for thyroid cancer is still limited due to the heterogeneity of tumor subtypes [7]. Identifying a tumor subtype-specific weakness would help develop additional therapeutic strategies.

Growing evidence supports the significance of mitochondrial metabolism for tumor cell survival and proliferation. We recently demonstrated that the mitochondrial molecular chaperone mortalin [also known as heat shock protein family A member 9 (HSPA9) or glucose-regulated protein 75] protects tumor cells from mitochondrial death caused by bioenergetic and redox stresses [8–10]. We showed that mortalin is upregulated in thyroid cancer and that mortalin depletion can effectively suppress different thyroid tumor cell lines *in vitro* and *in vivo* [8,11]. Importantly, mortalin overexpression also facilitates the survival of other tumor types, including pancreatic cancer and melanoma [9,10,12], breast cancer [13], lung cancer [14], and colon cancer [15]. Despite the potential of mortalin as a candidate therapeutic target and prognostic marker of cancer, the mechanism that increases its expression in the disease has been unclear.

Estrogen-related receptor alpha (ESRRA) is a transcription factor that belongs to the estrogen-related receptor family, a group of orphan nuclear receptors expressed mainly in metabolically active tissues [16]. ESRRA regulates transcriptions of various enzymes involved in glycolysis, tricarboxylic acid cycle, and oxidative phosphorylation [17]. ESRRA also facilitates tumor progression through physically or functionally interacting with different tumor promoters such as hypoxia-inducible factor [18,19], Myc [20], and transforming growth factor-β [21]. However, its relationship with mortalin has been unknown. ESRRA has been proposed as a therapeutic target in esophageal cancer [22], breast cancer [23–26], bladder cancer [27], oral squamous cell cancer [28], and prostate cancer [29]. Nevertheless, the role of ESRRA in thyroid cancer needs to be established.

In this study, we tested a hypothesis that ESRRA promotes thyroid tumor cell survival by increasing mortalin expression through transcription. Employing a comprehensive analysis of RNA-sequencing (RNA-seq) datasets from thyroid cancer patients, molecular analyses of *HSPA9* DNA promoter, and *in vitro* and preclinical studies of human thyroid tumor lines, we demonstrate that ESRRA directly regulates *HSPA9* transcription to facilitate tumor cell survival in follicular cell-, but not C cell-, originated thyroid cancer subtypes. Our patient sample analysis and preclinical studies also suggest a vital significance of the ESRRA/mortalin axis in tumors with oncocytic features.

Results

ESRRA and *HSPA9* are correlatively expressed in thyroid cancer in a tumor subtype- and tumor cell origin-specific manner

To determine the molecular mechanism underlying mortalin upregulation in cancer, we searched, using R2 Genomics Analysis and Visualization Platform [12], the TCGA patient mRNA datasets (11033 patients, 33 cancer types) for the transcription factors expressed in correlation with *HSPA9*. This screening identified *ESRRA* as one of the top candidates (Fig. 1A and Fig. S1), revealing that the *ESRRA*-*HSPA9* correlation is higher in thyroid cancer than other common cancer types, including carcinomas of prostate, lung, colon, and breast ($R = 0.571$, $p = 3.53e\text{-}48$, Fig. 1B). Notably, the Kaplan-Meier plots, generated by Gepia [30], based on the TCGA thyroid cancer datasets revealed that high *ESRRA* or *HSPA9* mRNA levels in the tumor are correlated with poor patient survival (Fig. 1C), suggesting a potential significance of these genes in the pathogenesis of thyroid cancer.

The TCGA thyroid cancer study was conducted on PTC [31]. To explore other thyroid cancer subtypes, we analyzed the *ESRRA*-*HSPA9* correlation using additional patient data available at Seoul National University Hospital (SNUH) in South Korea, which included PTC (n = 129), FTC (n = 35), ATC (n = 26), OCA (n = 7), and MTC (n = 27) [32,33], and the OCA data (n = 49) published by Chan group previously [34]. Our analysis of these data confirmed the *ESRRA*-*HSPA9* correlation detected in the TCGA data for PTC while revealing a tumor subtype- and cell type-specific correlation. Briefly, we found that *ESRRA* is positively correlated with *HSPA9* in follicular cell-originated PTC, FTC, OCA, and ATC, as well as in normal thyroid tissues (Fig. 1D). Our meta-analysis on these RNAseq datasets for each subtype consistently indicated the *ESRRA*-*HSPA9* correlation in follicular cell-originated tumor subtypes (Fig. 1E). Moreover, our IHC analysis of follicular cell-originated

patient tumor samples revealed that tumors exhibiting high ESRRA IHC positivity express high *HSPA9* mRNA levels (Fig. 1F). However, in contrast, *ESRRA* was not correlated with *HSPA9* in MTC, which is C cell-originated tumor (Fig. 1D). ESRRB and ESRRG often show complementary functions of ESRRA [35]. We found that these isoforms are differentially expressed in the same datasets (Fig. S2A), that *ESRRA* is negatively correlated with *ESRRB* while uncorrelated with *ESRRG* (Fig. S2B), and that, unlike *ESRRA*, these isoforms are not correlated with *HSPA9* in any tumor subtype in the datasets (Fig. S2C to S2E). These data suggested that ESRRA and mortalin expression has a cancer type- and cell type-specific correlation, leading us to hypothesize that ESRRA determines mortalin expression levels in follicular cell-originated tumor subtypes.

Depletion or inhibition of ESRRA suppresses thyroid tumor cell survival by inducing caspase-dependent apoptosis

To determine the role of ESRRA in thyroid tumor cells, we examined the effects of ESRRA depletion or inhibition in a panel of human thyroid cancer cell lines derived from PTC (TPC1 and BCPAP), FTC (FTC133), OCA (XTC.UC1), ATC (8505C) and MTC (TT and MZ-CRC-1). ESRRA knockdown using different lentiviral small hairpin RNA (shRNA) constructs consistently and significantly suppressed the viability of these cell lines by increasing cell death, as determined by TO-PRO3 assays (Fig. 2A; BCPAP results shown in Fig. S3A). Consistent with this, Western blotting revealed that ESRRA knockdown robustly induced the cleavage of lamin A in all these cell lines although it increased the cleavage of poly (ADP-ribose) polymerase (PARP) in TPC1, BCPAP, and FTC133 cells (Fig. 2B and Fig. S3B). The cleavage of lamin A and PARP is a surrogate marker for caspase-dependent apoptosis [36]. Indeed, as determined by the annexin V/propidium iodide co-staining in TPC1 and FTC133 cells, ESRRA knockdown induced apoptotic cell death, which was completely abrogated by the pan-caspase inhibitor, ZVAD (Fig. 2C). This inhibitor also abrogated ESRRA knockdown-induced cleavage of lamin A in these cells (Fig. 2C). However, ESRRA knockdown induced varied effects on the cell cycle inhibitors, $p16^{INK4a}$, $p21^{CIP1}$, and $p27^{KIP1}$ (Fig. 2B and Fig. S3B), while not markedly affecting the cell cycles, as determined in TPC1, BCPAP, FTC133 and 8505C cells (Fig. 2D). Moreover, when tested by XCT790, a highly selective ESRRA inhibitor that promotes proteasomal degradation of ESRRA [37,38], the follicular cell-originated cell lines exhibited lower IC_{50} values than the C cells-originated MTC lines, TT and MZ-CRC-1 (Fig. 2E). However, this inhibitor decreased ESRRA protein levels effectively in all these cell lines (Fig. S4). Importantly, the exogenous expression of an *ESRRA* gene engineered to avoid shESRRA#1 (hereafter referred to as ESRRA*) significantly abolished shESRRA#1-induced viability loss and lamin A cleavage, as determined in TPC1, FTC133, and 8505C cells (Fig. 3A, 3B, and Fig. S5A), confirming the specificity of the ESRRA knockdown effects. These data suggest that ESRRA has a role in facilitating thyroid tumor cell survival by suppressing caspase-dependent apoptosis and its role may be more important in the tumor cells originated from follicular cells than C cells.

ESRRA knockdown decreases mortalin levels in follicular cell-, but not in C-cell-, originated tumor cells, and mortalin overexpression rescues them from ESRRA depletion

We sought to determine whether mortalin has a role in mediating the effects of ESRRA in thyroid tumor cells. Intriguingly, ESRRA knockdown decreased mortalin protein levels

in the follicular cell-originated tumor cell lines, but not in the C-cell originated TT (Fig. 2B), which is consistent with the contrasting correlation of *ESRRA* and *HSPA9* in thyroid tumors of these origins (Fig 1C). ESRRA* overexpression restored mortalin levels in TPC1, FTC133, and 8505C cells depleted of ESRRA, confirming the specificity between ESRRA and mortalin (Fig. 3A and Fig. S5A).

Given these data, we determined whether an ectopic overexpression of mortalin can compensate for ESRRA deficiency in these tumor cells. Indeed, mortalin overexpression substantially rescued these tumor cells from the cell death induced by ESRRA knockdown (Fig. 3B). Mortalin overexpression also substantially abrogated ESRRA knockdown-induced lamin A cleavage and decreases in cytochrome C oxidase subunit IV (COX IV) levels, a surrogate marker for mitochondrial integrity [39], in these cells (Fig. 3B and Fig. S5B). These rescue effects of mortalin overexpression are quite comparable to those of ESRRA overexpression in these ESRRA-depleted cells seen in Fig. 3A, and Fig. S5A. These data suggest that mortalin might be a downstream effector of ESRRA in facilitating tumor cell survival and mitochondria integrity for follicular cell-originated tumor cells.

ESRRA binds to the DNA promoter of *HSPA9*

Consistent with its effect on cellular mortalin levels, ESRRA knockdown also decreased *HSPA9* mRNA levels in TPC1, FTC133, and 8505C cells, but not in TT cells, as determined by the qPCR analysis (Fig. 4A). These decreases were abrogated upon ESRRA* overexpression in the cells, confirming the specificity of the knockdown effects (Fig. 4A). ESRRA binds to a conserved DNA element known as ESRRA response element (ERRE) in the promoter region of its target genes [40]. A genome-wide ESRRA ChIP-sequencing screening revealed a putative ERRE site in mouse *Hspa9* [41], and we found that this site is conserved in humans and other higher species (Fig. 4B). As predicted by TRAP web tool [42], this putative ERRE is located between −377 and −366 base pair (bp) upstream of the transcription initiation site of human *HSPA9*, and this site (corresponding to 4501–4700 bp) displayed the highest affinity score among the five potential sites identified within 5000 bp upstream of the initiation site (Fig. 4C). Given this information, we determined whether ESRRA can directly bind to the human *HSPA9* promoter region containing the top-scored putative ERRE in FTC133 and TT cells, using the previously established ESRRA ChIP protocol and control oligomers for ESRRA binding [40]. Our data showed that *HSPA9* promoter was highly enriched in the ChIP fraction pulled by an ESRRA-specific antibody in FTC133 cells (Fig. 4D, top panel), and that this enrichment was significantly abrogated upon ESRRA knockdown (Fig. 4E and 4F). These data demonstrate that ESRRA can directly bind to the DNA promoter of *HSPA9*. In contratst, *HSPA9* promoter was not signficantly enriched in the ChIP fraction from TT cells (Fig. 4D, bottom panel). These data are consistent with the contrasting effects of ESRRA knockdown in these cell lines.

ESRRA regulates *HSPA9* transcription through a putative ERRE in the *HSPA9* promoter

To determine whether ESRRA regulates *HSPA9* transcription and, if so, whether the putative ERRE located between −377 and −366 bp is necessary for this regulation, we generated a series of luciferase promoter-reporters containing DNA fragments spanning −1,259 bp to +22 bp and −401 bp to +22 bp of human *HSPA9* promoter, referred to hereafter as p1259

and p401, respectively (Fig. 5A). We mutagenized the putative ERRE, using a previously reported algorithm [43], to disable its recognition by ESSRA (Fig. 5A). These reporters were examined in HEK293 cells that express wild type ESRRA or its DNA-binding domain mutant (DBDm) [44], depicted in Fig. 5B in comparison with the positive control reporter 3XERRE (3 repeats of validated ERRE) [45] and the negative pGL2 control. We found that both p1259 and p401 expressed the luciferase activity highly in cells expressing wild-type ESRRA, but not in cells expressing DBDm (Fig. 5C and 5D). Consistent with this data, the mutagenesis disabling the putative ERRE nullified the ability of these reporters to express the luciferase activity in response to ESRRA overexpression (Fig. 5C and 5D). To substantiate this observation, we designed a lentiviral CRISPR/Cas 9 sgRNA system targeting this ERRE (sgERRE, illustrated in Fig. 5E) and disrupted the endogenous *HSPA9* promoter region containing this element. CRISPR/Cas9 is known to typically generate deletions less than 30 bp or small insertions of 1 to a few bp in size [46]. Indeed, the lentiviral-sgERRE substantially suppressed cell viability and mortalin expression, at protein and mRNA levels, in FTC133 and 8505C cells when compared with the control sgRNA lentivirus (Fig. S6A to S6C). Moreover, the ectopic mortalin expression substantially rescued these cells from the sgERRE infection (Fig. 5F, 5G, and S6D), supporting the mortalin specificity of these sgERRE effects. Together, these data strongly suggest that ESRRA indeed regulates *HSPA9* transcription and mediates its regulation through the putative ERRE in the *HSPA9* promoter.

OCA exhibits higher ESRRA expression and activity than other thyroid tumor subtypes

The transcriptional activity and biological significance of ESRRA cannot be predicted simply by its protein levels but requires determining the expression of its defined target genes [22–25,47]. We systemically analyzed ESRRA expression and activity in the patient samples and data for follicular cell-originated tumor subtypes. First, our IHC data revealed that ESRRA protein levels are high in OCA relative to other follicular cell-originated tumor subtypes and normal thyroid tissues (Fig. 6A and 6B). OCA also exhibited the highest mortalin protein levels (Fig. 6A and 6B). Second, our heatmap analysis of the patient data for 120 ESRRA target genes, previously identified for determining ESRRA activity [23–25], revealed that these genes are thyroid histology-specifically expressed (Fig. 6C; the heatmap for individual patient grouped by tumor subtypes shown in Fig. S7). Strikingly, our data correlated relatively high expression of 79 genes (Cluster 1) and 41 genes (Cluster 2) with OCA and ATC, respectively (Fig. 6C and 6D). Further, our data indicated that the Cluster 1 and 2 genes might be expressed in a negatively correlated manner in thyroid epithelium ($p < 0.0001$, Fig. 6E).

Subsequently, our Kyoto Encyclopedia of Genes and Genomes (KEGG) and the Gene Ontology (GO) enrichment analyses, using ENRICHR [48], revealed that the gene clusters 1 and 2 are associated with different cellular processes (Fig. 6F, complete list in Table S1). For example, the Cluster 1 genes were mainly associated with mitochondrial processes, which is consistent with the role of ESRRA in regulating mitochondrial metabolism [49]. In contrast, the Cluster 2 genes were associated with other various pathways. These data suggest that ESRRA may have a thyroid tumor subtype-specific role. Mortalin belongs to the Cluster 1 gene group (Fig. 6C). Intriguingly, the mortalin-associated cellular processes and pathways

(Table S2), which we recently identified by proteomic analysis of mortalin interactome [9], exhibited a significantly positive correlation by adjusted p values (in −log10 scale) with the Cluster 1 gene set-associated pathways but no significant correlation with the Cluster 2 gene set-associated pathways ($p = 0.0002$ for Cluster 1 and $p = 0.3574$ for Cluster 2; Fig. 6G). Therefore, ESRRA and mortalin might have a higher functional overlap in OCA than in other tumor subtypes.

A novel molecular subtyping based on ESRRA signature gene expression

Because the data above suggested that the ESRRA signature scoring can reveal a novel molecular feature in thyroid cancers, we performed an unsupervised hierarchical clustering algorithm on our patient data based on the ESRRA signature genes, irrespective of the histology. Indeed, we found that the patient samples can be clustered into two distinct molecular subtypes, namely Type 1 and Type 2 (Fig. 7A). We confirmed the robustness of this molecular subtyping by fitting a random forest supervised machine learning algorithm to classify the Type 1 and Type 2 subtypes and evaluating them by receiver operating characteristic (ROC) analysis with leave-one-out cross-validation with ROC analysis (LOOCV AUC = 0.997, Fig. 7B). Strikingly, entire OCA and ATC samples were exclusively classified as Type 1 and Type 2, respectively, according to this molecular subtyping (Fig. 7C). Meanwhile, PTC, FTC, and the non-tumor tissue samples included both types, wherein the non-tumor tissue and FTC samples contained similarly higher Type 1 distributions whereas PTC samples contained a higher Type 2 distribution (Fig. 7C). We found that the Type 1 patient samples expressed the Cluster 1 genes higher whereas the Type 2 samples expressed the Cluster 2 genes higher, irrespective of their histology (Fig. 7D). Using the random forest algorithm, we also ranked these genes, wherein a higher rank meant a larger effect in distinguishing Type 1 and Type 2, to identify 30 candidate biomarkers for predicting these molecular subtypes (Fig. 7E). These data demonstrate that a novel molecular subtyping based on the ESRRA signature genes can refine conventional thyroid histology subtyping.

ESRRA depletion suppresses xenografts of XTC.UC1 and FTC133 in mice

We sought to evaluate the preclinical significance of ESRRA for thyroid cancer, especially for those that exhibit oncocytic features because the data above suggested a relatively high significance of ESRRA for OCA. To this end, we used XTC.UC1, the only human OCA cell line [50], and FTC133, which exhibits a metabolic feature similar as oncocytic tumors [51]. Both cell lines expressed ESRRA higher than other follicular cell-originated tumor lines (Fig. 2E) and were sensitive to ESRRA knockdown in vitro (Fig. 2A and 2B). When XTC.UC1 cells infected with the lentiviral shESRRA#1 were injected into immune-compromised mice, their tumors grew more slowly than those infected with pLL3.7 control virus (Fig. 8A to 8C). Similarly, ESRRA knockdown significantly suppressed the growth of FTC133 xenografts in mice (Fig. 8D), and it also prolonged mice survival (Fig. 8E). Both cell line xenografts did not affect animal body weights regardless of the virus used (Fig. S8). Although the effects were varied in different mice, ESRRA knockdown also decreased protein (Fig. 8F, densitometry in 8G) and mRNA (Fig. 8H) levels of mortalin in the tumors of XTC.UC1 and FTC133. These effects are consistent with the *in vitro* effects of ESRRA knockdown in these cell lines (Fig. 2B). Lastly, we tested Compound 29 (C29), an advanced ESRRA

inhibitor [52], in the XTC.UC1 xenograft model. Consistent with ESRRA knockdown, C29 significantly suppressed the growth of XTC.UC1 xenografts in mice (Fig. 8I to 8K), and decreased mRNA (Fig. 8L) and protein (Fig. 8M, densitometry in 8N) levels of mortalin. Together, these data suggest that ESRRA may have potential as a therapeutic target for thyroid cancer.

Discussion

Our findings reveal a novel ESRRA-mortalin axis in thyroid cancer. Our RNA-seq and IHC analyses of patient tumors have revealed a positive correlation between ESRRA and *HSPA9* RNA levels, which is specific to the follicular cell-originated tumors. This correlation led us to reveal a functional relationship between mortalin and ESRRA in the tumors. Mechanistically, our data suggest that ESRRA increases mortalin levels in the follicular cell-originated tumor cells by directly binding to an ERRE located in the *HSPA9* promoter and, subsequently, facilitating *HSPA9* transcription. In stark contrast, the C cell-originated MTC did not show any correlation between *ESRRA* and *HSPA9*, and ESRRA knockdown did not affect mortalin levels in MTC cells. These data suggest that ESRRA regulates mortalin expression in thyroid cancer in a tumor subtype-specific manner. Moreover, our study has identified the relatively high significance of the ESRRA-mortalin axis in OCA and a novel molecular signature that contrasts oncocytic-like subtypes and ATC in stark based on ESRRA target gene expression.

The differential mortalin regulation by ESRRA between the tumors originated from follicular cells and the C cells may be attributed to a critical difference determined by these proteins in these tumor types, probably due to a unique biological characteristic in the thyroid gland or a tumor subtype-specific alteration. For example, follicular cells exhibit typical epithelial cell features and produce thyroid hormones, whereas the less abundant C cells exhibit neuroendocrine features secreting calcitonin [53]. Nevertheless, the molecular mechanism underlying this dichotomy between these cells is yet to be identified. Given that ESRRA is a key regulator of metabolism, different metabolic features in these cells or their tumors may underlie the differential regulation. Indeed, MTC exhibits relatively high fatty acid levels [54], relatively low expression of hexokinase 2, the first rate-determining enzyme in glycolysis [55], and carbonic anhydrase IX, which regulates hydrogen ion flux and is a hypoxia-inducible factor target activated by the oncogenic kinase REarranged-during-Transfection in MTC [55,56]. Given that ESRRA and mortalin are also crucial for the survival of MTC cells (this study and [8]), we speculate that these proteins might facilitate MTC cell survival via independent mechanisms.

Our patient data show that OCA exhibits relatively high ESRRA and mortalin expression. Our *in vitro* and preclinical studies suggest that ESRRA targeting can effectively suppress OCA and oncocytic variant tumor cells. OCA is a relatively aggressive thyroid tumor with a higher incidence of distant metastases [3,57], and there is a significant challenge in diagnosing and treating the tumor [58]. OCA is characterized by abnormally high amount of dysfunctional mitochondria and mutations in the mitochondrial genome [34,59,60]. This mitochondrial abnormality is suspected as a compensatory effect to complex I dysfunction, possibly cellular effort to increase mitochondrial biogenesis and oxidative metabolism [61,62].

However, patient-derived OCA cells exhibit low mitochondrial respiration but high rates of glycolysis, indicating compensation through the Warburg effect [63,64]. These alterations are in line with the upregulation of ESRRA and mortalin in the tumor, as both proteins play an important role in mitochondrial metabolism. The present study suggests that the ESRRA-mortalin axis is especially important in OCA and certain oncocytic variant thyroid tumors, proposing the pathway as a candidate therapeutic target for these tumors.

The present study demonstrates that ESRRA differentially regulates its target genes in follicular cell-derived thyroid cancers. Notably, OCA and ATC exhibited contrasting expression patterns of ESRRA target genes, which are clustered into two gene signature groups, Cluster 1 and Cluster 2. These ESRRA signatures enabled us to classify thyroid follicular epithelium into the Type 1 and Type 2 molecular subtypes, wherein OCA contains only the Type 1 subtype with the highest Cluster 1 gene score, whereas ATC contains only the Type 2 subtype with the highest Cluster 2 gene score. Because other tumor subtypes and normal follicular epithelium contain these subtypes in a mixed manner along with varied cluster scores, it is conceivable that the differential expression of the cluster genes indicates a differentiation or dedifferentiation program that determines the path of oncogenesis. For example, the Type 2 population and the cluster 2 score increased in the order of non-tumor tissues, PTC, and ATC, which is consistent with the posit that ATC arises from PTC [65]. Similarly, expression of the Cluster 1 genes may enrich the Type 1 population and facilitate the development of OCA and oncocytic PTC and FTC variants (illustrated in the graphic abstract). Importantly, *ESRRA* is a biomarker for the Non–*BRAF*–Non–*RAS* molecular subtype of thyroid cancer, which mainly includes OCA and certain oncocytic PTC and FTC variants that exhibit altered tricarboxylic acid cycle and oxidative phosphorylation [32]. The novel molecular subtyping identified in this study advances the use of ESRRA to refine current molecular subtypes in thyroid cancer.

In summary, our study reveals a novel regulatory and functional relationship between ESRRA and mortalin in follicular cell-originated thyroid cancer, providing a novel insight into the mechanism underlying mortalin upregulation in cancer. Based on our findings, we propose that ESRRA is a tumor-type-specific regulator of mortalin expression and that ESRRA facilitates the survival of thyroid tumor cells through differential transcriptional programs specific to tumor cell origin. In support of this notion, differential gene regulation by ESRRA was also detected in a manner specific to different breast cancer subtypes [24,26,44,66]. How does ESRRA regulate diverse transcription? While being an orphan nuclear factor, ESRRA regulates gene expression in cooperation with co-transcription factors, including peroxisome proliferator-activated receptor γ co-activators 1α and 1β, peroxisome proliferator-activated receptor γ co-activator-related protein 1, nuclear receptor co-repressor 1, and nuclear-receptor-interacting protein 1 [49,67]. These co-regulators determine the target specificity of ESRRA [49]. A future study remains on whether ESRRA utilizes these co-regulators differentially in thyroid tumors.

Materials and Methods

Ethics statement

This study was approved by the Institutional Review Board (IRB) of Seoul National University Hospital (SNUH) and Medical College of Wisconsin (MCW) in accordance with the Declaration of Helsinki (approved ID: H-1108-041-372 and H-2303-179-1418). Written informed consent was obtained from each subject.

RNA sequencing and data analysis

The RNA sequencing (RNA-seq) analyses were performed using TCGA data (https://portal.gdc.cancer.gov/) and the data previously published by SNUH [32,33] and the Chan group [34]. TCGA data include 505 PTCs with 59 partially matched normal thyroid tissues, and SNUH-2 data include 224 thyroid cancer samples (129 PTCs, 35 FTCs, 7 OCAs, 26 ATCs, and 27 MTCs) and 90 partially matched normal tissue samples. The majority of MTC samples were collected from patients at SNUH. The MTC data, labeled SNUH-1 dataset, were jointly generated by the Korea Research Institute of Bioscience and Biotechnology and Chungnam National University. The sequenced paired-end reads were aligned to GRCh38 human reference genome using STAR 2-pass method [68,69] after trimming by Trimmomatic [70]. The read counts and TPM values were quantified by RSEM [71] with default parameters. To analyze the 120 ESRRA signature genes [23–25], their read counts were normalized using the variance stabilizing transformation in the DESeq2 package and visualized using R package ComplexHeatmap [72]. Clustering analysis for ESRRA signature genes was performed by hierarchical clustering algorithm. The ESRRA Cluster 1 and Cluster 2 scores for each sample were calculated by taking the average normalized expression level from each cluster respectively. Patient samples were clustered into Type 1 and Type 2 by hierarchical clustering algorithm. To further identify top molecular markers that distinguish Type 1 and Type 2 patient samples, we fitted a random forest machine learning algorithm (R package randomForest [73]) and performed a receiver operating characteristic (ROC) curve analysis with leave-one-out cross-validation (LOOCV) to verify the robustness of this classification. The area under the curve (AUC) was calculated to evaluate the performance. R package randomForest and ROCR were used for fitting the random forest algorithm and ROC curve, respectively. Mean decrease Gini impurity measurement was used to rank efficiently the ESRRA signature genes that contributed to the Type 1 and Type 2 classification and to identify the top molecular markers for this classification.

Tissue microarray and immunohistochemistry

Thyroid tissue microarrays were constructed as previously described [74]. Briefly, thyroid tissue samples from patients who underwent thyroidectomy were obtained from the surgical pathology files of the Departments of Pathology at Seoul National University Boramae Medical Center and Seoul National University Hospital. Hematoxylin and eosin (H&E) stained thyroid tissues were examined using slides by two independent pathologists, and the appropriate paraffin blocks were chosen. Core thyroid tissue samples (2 mm in diameter) were taken from the individual paraffin-embedded thyroid tissue donor blocks and arrayed on the recipient paraffin blocks. Using tissue microarrays, 1246 and 314 samples were subjected to IHC staining for ESRRA (191 thyroids, 825 PTCs, 156 FTCs,

20 OCAs, and 54 ATCs) and mortalin (14 thyroids, 181 PTCs, 71 FTCs, 2 OCAs, and 46 ATCs), respectively. IHC staining was performed on formalin-fixed paraffin-embedded tissue sections 4 μm thick using an automated immunostainer (Leica Microsystems, Milton Keynes, UK). Briefly, the slides were heated for 20 min at 100 °C in epitope retrieval solution, pH 9.0 (Leica Microsystems). The slides were then incubated with a monoclonal rabbit anti-human ESRRA antibody (Cell Signaling, Danvers, MA, #13826) and monoclonal mouse anti-human mortalin antibody, D-9 (Santa Cruz Biotechnology, Santa Cruz, CA, #sc-133137). Staining intensity (nuclear staining for ESRRA and cytoplasmic staining for mortalin) was scored as 0, negative; 1, weak; 2, medium; and 3, strong.

Cell culture and Reagents

The human thyroid cancer cell lines TPC1 (ATCC, Manassas, VA), BCPAP (ATCC), 8505C (ATCC), and C643 (ATCC) were maintained in RPMI 1640 (Invitrogen, Thermo Fisher Scientific, Waltham, MA, #11875) supplemented with 10% heat-inactivated fetal bovine serum (FBS, Gibco, Thermo Fisher Scientific, #16000–044) and 100 U of penicillin-streptomycin (Gibco, #15140) per mL. FTC133, XTC.UC1 and MZ-CRC-1 were maintained in DMEM (Gibco, #11965) supplemented with 10% heat-inactivated FBS and 100 U of penicillin-streptomycin per mL. TT was maintained in DMEM supplemented with 16% heat-inactivated FBS and 100 U of penicillin-streptomycin per mL. HEK293T and HEK293 were maintained in DMEM supplemented with 10% bovine growth serum (Hyclone, Cytiva, Muskegon, MI, #SH30541.03). All experiments were performed using cells within ten passages from the acquisition point. 3-[4-(2,4-Bis-trifluoromethyl benzyloxy)-3-methoxyphenyl]-2-cyano-N-(5-trifluoromethyl-1,3,4-thiadiazol-2-yl)acrylamide (XCT790) and carbobenzoxy-valyl-alanyl-aspartyl-[O-methyl]-fluoromethylketone (ZVAD) were purchased from Tocris (Minneapolis, MN, #3928) and Selleckchem (Houston, TX, #S7023), respectively. C29 was purchased from MilliporeSigma (St. Louis, MO, #533659).

Cell viability and cell cycle analyses

Cell viability was determined by flow cytometry of cells stained with the fluorescent DNA intercalator Thiazole Red (TO-PRO®3, Invitrogen, #T3605) using Guava EasyCyte flow cytometry system (MilliporeSigma, St. Louis, MO, #05005007). To determine apoptosis, cells were co-stained with Annexin V (Invitrogen, #A35122) and 7-Aminoactinomycin D (7-AAD) (Invitrogen, #00–6993-50) according to manufacturer's instructions, and then flow cytometry was performed using BD® LSR II Flow Cytometer (Franklin Lakes, NJ). To analyze cell cycle, cells were stained with propidium iodide (PI, Invitrogen, #P1304MP) and flow cytometry was performed using the Guava EasyCyte flow cytometry system, as previously described [75]. Flow cytometry data were analyzed by FCS EXPRESS software (De Novo Software, Los Angeles, California). To determine the IC_{50} value, cells in 96-well plates were fixed in formaldehyde (Fisher Chemical, Thermo Fisher Scientific, #BP531), stained with 0.05% Crystal Violet (Fisher Chemical, #C58125) for 30 minutes, washed with water three times, air-dried, and incubated in 200 μL of methanol (VWR Chemicals BDH®, Radnor, PA #BDH1135) for 10 min at room temperature before measuring absorbance at 540 nm.

Immunoblotting

Cells were harvested in lysis buffer containing 62.5 mM Tris-HCl (pH 6.8), 2% sodium dodecyl sulfate, protease inhibitor, and phosphatase inhibitor cocktails 2 and 3 (MilliporeSigma, #P8340, P5726, and P0044, respectively). Protein concentration was determined using the Pierce™ BCA Protein Assay Kit (Pierce, Thermo Fisher Scientific, #23227). Protein samples were resolved on the sodium dodecyl sulfate (SDS)-polyacrylamide gel electrophoresis and transferred to the polyvinylidene difluoride membrane filter (Bio-Rad, Hercules, CA, #1620177). After transfer, membranes were blocked in a buffer containing 0.1 M Tris (pH 7.4), 0.9% NaCl, 0.1% Tween 20, and 5% nonfat dry milk for 1 h at 25 °C. Membranes were then incubated with the appropriate antibody overnight at 4 °C with agitation at the following dilutions: ESRRA (Cell Signaling, #13826) 1:1000; PARP (Cell Signaling, #9542) 1:2000; cleaved lamin A (Cell Signaling, #2035) 1:1000; cytochrome c oxidase subunit IV (COX IV, Cell Signaling, #4850) 1:2000; mortalin (Santa Cruz Biotechnology, #sc-133137) 1:5000; $p21^{CIP1}$ (Santa Cruz Biotechnology, #sc-56335) 1:1000, $p27^{KIP1}$ (Santa Cruz Biotechnology, #sc-1641) 1:1000; $p16^{INK4A}$ (BD Bioscience, San Jose, CA, #554079) 1:1000 and β-actin (MilliporeSigma, #A2228) 1:5000. Chemiluminescence signals of immunoblots were visualized by SuperSignal West Pico and Femto chemiluminescence kits (Pierce, #34079 and #23227), captured by ChemiDoc XRS+ (Bio-Rad), and analyzed by Image Lab software (Bio-Rad) for densitometry.

RNA interference, CRISPR/Cas 9, and recombinant lentiviral constructs

ESRRA was depleted using the lentiviral shRNA expression systems pLL3.7-shESRRA#1, shESRRA#2, and shESRRA#3 that target three different coding regions of human *ESRRA* GAGAGGAGTATGTTCTACTAA, AAGACAGCAGCCCCAGTGAA and CTACCACTATGGTGTGGCA, respectively. Briefly, complementary oligos with HpaI/XhoI sites were ordered from Thermo Fisher Scientific, annealed, and ligated to HpaI/XhoI sites of pLL3.7 [75]. To construct the lentivirus expressing N-terminally HA-tagged ESRRA (pHAGE-HA-ESRRA), *ESRRA* coding region was amplified from pCMV flag ESRRA (Addgene, Watertown, MA, #10975) [76] using AccuPrime™ Pfx SuperMix (Invitrogen, #12344040) and the primers, TTATCCGCTAGCTCCAGCCAGGTGGTGGGCATTGAGCC and TTTCTGGGATCCTCAGTCCATCATGGCCTCGAGCATC. Obtained *ESRRA* cDNA was ligated to the NheI/BamHI sites of pHAGE-HA [75]. The non-shESRRA#1-targetable pHAGE-HA-ESRRA* was generated using the QuikChange Lightning site-directed mutagenesis kit (Agilent, Santa Clara, CA, #210518) and the primers, GGCTGGAGCGAGAGGAATACGTACTACTAAAGGCCTTGG and CCAAGGCCTTTAGTAGTACGTATTCCTCTCGCTCCAGCC. The pHAGE expression systems for mortalin were previously described [75]. LentiCRISPR v2-sgControl (sgCont) was a gift from Dr. Boyi Gan [77] (Addgene # 125836). The lentiviral sgERRE was generated by ligated the annealing product of CACCGAGGAAAGACTCAAGGTCACA and AAACTGTGACCTTGAGTCTTTCCTC to LentiCRISPR v2, which was a gift from Dr. Feng Zhang [78] (Addgene # 52961). Lentiviruses were generated from HEK293T cells and used, as we previously described [79].

Quantitative real time-PCR (qPCR)

Total RNA was extracted using TRIzol® reagent (Invitrogen, #15596026) and reverse-transcribed using Superscript III (Invitrogen, #18080093), dNTP (Invitrogen, #18427013), and oligo(dT)$_{12–18}$ primer (Invitrogen, #18418012), according to the manufacturer's instruction. qPCR was performed using the PerfeCTa® SYBR® Green FastMix®, Low ROX™ (Quantabio, Beverly, MA, #95074–250) and Stratagene MX3005P instrument (Agilent). TTATCCGCTAGCAATGAGCCCACAGCTGCTGCTCTTGCC and TTTCTGGGATCCTTACACATCCGTGACATCGCCGGCC are primers for *HSPA9*. GTCCTCTCCCAAGTCCACAC and GGGAGA CCAAAAGCCTTCAT are primers for *ACBT*.

Luciferase reporter assays

A DNA fragment spanning from −1259 base pair to +22 base pair of *HSPA9* promoter was PCR amplified from the genomic DNA of TPC1 cells, using AccuPrime™ Pfx SuperMix (Invitrogen, #12344040) and the primers GTAGTTGACATCCTGCCACC and CAGCTCGGCTGGCACTTATC, and cloned into TOPO-TA vector (Invitrogen, #K466040). To generate the luciferase reporter p1259, the *HSPA9* promoter in this TOPO vector was amplified using TTCGCCCTGGTACCTGACATCCT and GCCCTTCAGATCTGCTGGCACTT and was ligated into the KpnI/BgIII sites of pGL2 basic vector (Promega, Madison, WI, #E1641). To generate the luciferase reporter p401, a *HSPA9* promoter DNA fragment spanning from −401 to +22 was generated by PCR from p1259 using GGTACCGGTTCGCAATTTATCCCG and GCCCTTCAGATCTGCTGGCACTT, and then ligated into KpnI/BgIII sites of pGL2 basic vector. Putative ERRE sites in p1259 and p401 were mutated using the QuikChange Lightning site-directed mutagenesis kit, and the primers GCAATTTATCCCGTGCACAATTGAGTCTTTCC and GGAAAGACTCAATTGTGCACGGGATAAATTGC. To generate reporter cell lines, HEK293 cells were stably transfected with pGL2, 3XERRE (Addgene, #37851), p1259, or p401 with the wildtype or mutant ERRE together with pcDNA™3.1/Hygro(+) with 10:1 ratio in 6-well plates using 293Expresso™ Transfection Reagent (Excellgen, Waltham, MA, #EG-1089), and selected with 500 μg/mL hygromycin B (Invitrogen, #10687010) for 72 h. To measure the reporter activity, total cell lysates were extracted and analyzed using the Luciferase® Assay System (Promega, #E1960) according to the manufacturer's instructions. Data were normalized to total protein concentrations, measured by Bradford protein assay (Bio-Rad, #2000001).

Chromatin immunoprecipitation (ChIP) -qPCR

ChIP assay was performed as described previously [80] with minor modifications. Briefly, cells in 100 mm dishes were crosslinked with 1% formaldehyde for 10 min. Then, reactions were quenched by adding glycine to the 0.125 M final concentration (MilliporeSigma, #50046). Cells were washed, scraped, and lysed in the lysis buffer containing 20 mM Tris [pH 8.1], 5 mM PIPES, 85 mM KCl, and 0.5% NP40. Nuclei were then lysed in the lysis buffer containing 50 mM Tris-HCl [pH 8.1], 10 mM EDTA and 1% SDS. Chromatin was sonicated to an average size of approximately 500 base

pairs, diluted in 16.7 mM Tris buffer [pH 8.1] containing 0.01% SDS, 1% Triton X-100, 1.2 mM EDTA, 167 mM NaCl, and precleared with Dynabeads™ Protein A (Invitrogen, #10001D). Protein was quantified using Bradford assay (Bio-Rad). 1% of starting chromatin was used as input. Four hours of immunoprecipitations were performed using an ESRRA-specific antibody (Cell Signaling, #13826) and the control normal rabbit IgG (Cell Signaling, #2729). Immunoprecipitants were incubated at 67 °C for 4 h to reverse the formaldehyde crosslinking. DNA was then purified using the StrataPrep PCR Purification Kits (Agilent, #400771) and subjected to qPCR using the following primers. GTCTCCACCCATGTTTTCCG and ATGAAGGCCGTATCTCGGAC amplify −519 to −318 base pairs of *HSPA9* promoter in which the putative ERRE is present between −377 and −366 base pairs. CCATCCGAGTGGAATTTGAGTCCTAAAG and GAACCGTAGACCCAGTAGCCCCACAGAG were the positive control. GTGGCCCACAGGTGTCGCTCAAGTCTTC and GGATGCAGTGTCCTTCTCCCCCAGATTG were the negative control [40]. Percent input [81] and fold enrichment [82] were used to normalize ChIP-qPCR data.

Tumor xenografts

For ESRRA knockdown, a total of 4×10^6 cells harvested at 24 h post-infection with pLL3.7 or shESRRA#1 and suspended in 100 μL of Hank's balanced salt solution (Gibco, #14025) mixed with Extracellular Matrix Gel (MilliporeSigma, #E6909) at 1:1 ratio were inoculated subcutaneously into the rear flanks of 6-week-old female athymic nude (*nu*/*nu*) mice (The Jackson Laboratory, Bar Harbour, ME, #007850). Once palpable, tumors were measured using Vernier calipers twice a week. Tumor volumes were calculated using the formula: length × width × height × 0.5236. For C29 treatment, 4×10^6 cells were inoculated into mice as described above. When tumor volumes reached 50 mm^3, mice were randomized and sorted into 2 groups of 5 animals to achieve equal tumor size distribution in all treatment groups. Drugs dissolved in 100 μl vehicle (1:12 mixture of DMSO/15% β-cyclodextrin) were orally administered by gavage daily. The control group received only the vehicle, the C29 group received 30 mg drug/kg body weight/dose. Ethical endpoints were when tumors showed ulceration or their size reached 1200 mm^3. At the end of the experiments, animals were euthanized by CO_2 asphyxiation, and tumor tissues were harvested. All animal studies were performed according to protocols approved by the Institutional Animal Care and Use Committee at the Medical College of Wisconsin (AUA00001327).

Quantification and statistical analyses

All graphs represent the mean ± the standard deviation of biological triplicates' mean (SEM). Statistical significance was determined by one-way or two-way ANOVA, mixed effects model analysis with Bonferroni tests for multiple testing corrections, and Student's t-test using PRISM (Graph-Pad Software, La Jolla, CA) unless stated otherwise in the figure legend. IC_{50} values were determined by PRISM. Gene expression and patient survival datasets from the TCGA-thyroid carcinoma (THCA) study [31] were analyzed by R2 Genomics Analysis and Visualization Platform (http://r2.amc.nl) [12] and the Human Protein Atlas [83]. *p* values for the Kaplan-Meier curves were determined by the log-rank test. *p* values of < 0.05 were considered statistically significant. Meta-analysis was performed using the Fisher's method [84].

Supplementary Material

Refer to Web version on PubMed Central for supplementary material.

Acknowledgments

We thank Dr. Barry Nelkin (Johns Hopkins Medical Institute) for TPC1, BCPAP, FTC133, C643, 8505C, and TT; Dr. John A. Copland III (Mayo Clinic) for XTC.UC1; and Dr. Robert Gagel (MD Anderson) for MZ-CRC-1.

Financial support:

This work was supported by NIH/National Cancer Institute grants (R01CA138441 and R01CA269452) to J.P.

Data availability

All data needed to evaluate the conclusions in the paper are present in the paper and the Supplementary Materials.

Reference

1. National Cancer Institute: Surveillance, E., and End Results Program. ICD-O-3/WHO 2008. Vol. 2023.
2. Jung CK, Bychkov A & Kakudo K Update from the 2022 World Health Organization Classification of Thyroid Tumors: A Standardized Diagnostic Approach. Endocrinol Metab (Seoul) 37, 703–718 (2022). [PubMed: 36193717]
3. Chindris AM, et al. Clinical and molecular features of Hurthle cell carcinoma of the thyroid. J Clin Endocrinol Metab 100, 55–62 (2015). [PubMed: 25259908]
4. Kushchayeva Y, Duh QY, Kebebew E & Clark OH Prognostic indications for Hurthle cell cancer. World J Surg 28, 1266–1270 (2004). [PubMed: 15517492]
5. Coca-Pelaz A, et al. Hurthle Cell Carcinoma of the Thyroid Gland: Systematic Review and Meta-analysis. Adv Ther 38, 5144–5164 (2021). [PubMed: 34423400]
6. Kebebew E, Greenspan FS, Clark OH, Woeber KA & McMillan A Anaplastic thyroid carcinoma. Treatment outcome and prognostic factors. Cancer 103, 1330–1335 (2005). [PubMed: 15739211]
7. Nucera C Evolution of resistance to thyroid cancer therapy. Aging (Albany NY) 8, 1576–1577 (2016). [PubMed: 27575377]
8. Starenki D, Hong SK, Lloyd RV & Park JI Mortalin (GRP75/HSPA9) upregulation promotes survival and proliferation of medullary thyroid carcinoma cells. Oncogene 34, 4624–4634 (2015). [PubMed: 25435367]
9. Wu PK, et al. Mortalin (HSPA9) facilitates BRAF-mutant tumor cell survival by suppressing ANT3-mediated mitochondrial membrane permeability. Sci Signal 13(2020).
10. Wu PK, et al. Mortalin/HSPA9 targeting selectively induces KRAS tumor cell death by perturbing mitochondrial membrane permeability. Oncogene 39, 4257–4270 (2020). [PubMed: 32291414]
11. Starenki D, Sosonkina N, Hong SK, Lloyd RV & Park JI Mortalin (GRP75/HSPA9) Promotes Survival and Proliferation of Thyroid Carcinoma Cells. Int J Mol Sci 20(2019).
12. R2: Genomics Analysis and Visualization Platform
13. Na Y, et al. Stress chaperone mortalin contributes to epithelial-mesenchymal transition and cancer metastasis. Cancer Res 76, 2754–2765 (2016). [PubMed: 26960973]
14. Sun J, et al. Mortalin overexpression predicts poor prognosis in early stage of non-small cell lung cancer. Tumour Biol 39, 1010428317695918 (2017). [PubMed: 28349826]
15. Black JD & Rezvani K Heat Shock Protein 70s as Potential Molecular Targets for Colon Cancer Therapeutics. Curr Med Chem 23, 3171–3188 (2016). [PubMed: 27356538]
16. Giguere V, Yang N, Segui P & Evans RM Identification of a new class of steroid hormone receptors. Nature 331, 91–94 (1988). [PubMed: 3267207]

17. Huss JM, Garbacz WG & Xie W Constitutive activities of estrogen-related receptors: Transcriptional regulation of metabolism by the ERR pathways in health and disease. Biochim Biophys Acta 1852, 1912–1927 (2015). [PubMed: 26115970]
18. Ao A, Wang H, Kamarajugadda S & Lu J Involvement of estrogen-related receptors in transcriptional response to hypoxia and growth of solid tumors. Proc Natl Acad Sci U S A 105, 7821–7826 (2008). [PubMed: 18509053]
19. Hamidian A, von Stedingk K, Munksgaard Thoren M, Mohlin S & Pahlman S Differential regulation of HIF-1alpha and HIF-2alpha in neuroblastoma: Estrogen-related receptor alpha (ERRalpha) regulates HIF2A transcription and correlates to poor outcome. Biochem Biophys Res Commun 461, 560–567 (2015). [PubMed: 25912138]
20. Cai Q, Lin T, Kamarajugadda S & Lu J Regulation of glycolysis and the Warburg effect by estrogen-related receptors. Oncogene 32, 2079–2086 (2013). [PubMed: 22665055]
21. Chen Y, Zhang K, Li Y & He Q Estrogen-related receptor alpha participates transforming growth factor-beta (TGF-beta) induced epithelial-mesenchymal transition of osteosarcoma cells. Cell Adh Migr 11, 338–346 (2017). [PubMed: 27532429]
22. Dings MPG, et al. Estrogen-related receptor alpha drives mitochondrial biogenesis and resistance to neoadjuvant chemoradiation in esophageal cancer. Cell Rep Med 3, 100802 (2022). [PubMed: 36334593]
23. Chang CY, et al. The metabolic regulator ERRalpha, a downstream target of HER2/IGF-1R, as a therapeutic target in breast cancer. Cancer Cell 20, 500–510 (2011). [PubMed: 22014575]
24. Stein RA, et al. Estrogen-related receptor alpha is critical for the growth of estrogen receptor-negative breast cancer. Cancer Res 68, 8805–8812 (2008). [PubMed: 18974123]
25. Vernier M, et al. Inhibition of DNMT1 and ERRalpha crosstalk suppresses breast cancer via derepression of IRF4. Oncogene 39, 6406–6420 (2020). [PubMed: 32855526]
26. Vargas G, et al. ERRalpha promotes breast cancer cell dissemination to bone by increasing RANK expression in primary breast tumors. Oncogene 38, 950–964 (2019). [PubMed: 30478447]
27. Kim S, et al. Clinicopathological Profiling of LC3B, an Autophagy Marker, and ESRRA (Estrogen-related Receptor-alpha) in Muscle-invasive Bladder Cancer. Anticancer Res 38, 2429–2437 (2018). [PubMed: 29599373]
28. Tiwari A, Swamy S, Gopinath KS & Kumar A Genomic amplification upregulates estrogen-related receptor alpha and its depletion inhibits oral squamous cell carcinoma tumors in vivo. Sci Rep 5, 17621 (2015). [PubMed: 26639757]
29. Xu Z, et al. Nuclear receptor ERRalpha and transcription factor ERG form a reciprocal loop in the regulation of TMPRSS2:ERG fusion gene in prostate cancer. Oncogene 37, 6259–6274 (2018). [PubMed: 30042415]
30. Tang Z, et al. GEPIA: a web server for cancer and normal gene expression profiling and interactive analyses. Nucleic Acids Res 45, W98–W102 (2017). [PubMed: 28407145]
31. Cancer Genome Atlas Research, N. Integrated genomic characterization of papillary thyroid carcinoma. Cell 159, 676–690 (2014). [PubMed: 25417114]
32. Yoo SK, et al. Comprehensive Analysis of the Transcriptional and Mutational Landscape of Follicular and Papillary Thyroid Cancers. PLoS Genet 12, e1006239 (2016). [PubMed: 27494611]
33. Yoo SK, et al. Integrative analysis of genomic and transcriptomic characteristics associated with progression of aggressive thyroid cancer. Nat Commun 10, 2764 (2019). [PubMed: 31235699]
34. Ganly I, et al. Integrated Genomic Analysis of Hurthle Cell Cancer Reveals Oncogenic Drivers, Recurrent Mitochondrial Mutations, and Unique Chromosomal Landscapes. Cancer Cell 34, 256–270 e255 (2018). [PubMed: 30107176]
35. Giguere V Transcriptional control of energy homeostasis by the estrogen-related receptors. Endocr Rev 29, 677–696 (2008). [PubMed: 18664618]
36. Rosen A & Casciola-Rosen L Macromolecular substrates for the ICE-like proteases during apoptosis. J Cell Biochem 64, 50–54 (1997). [PubMed: 9015754]
37. Busch BB, et al. Identification of a selective inverse agonist for the orphan nuclear receptor estrogen-related receptor alpha. J Med Chem 47, 5593–5596 (2004). [PubMed: 15509154]
38. Lanvin O, Bianco S, Kersual N, Chalbos D & Vanacker JM Potentiation of ICI182,780 (Fulvestrant)-induced estrogen receptor-alpha degradation by the estrogen receptor-related

receptor-alpha inverse agonist XCT790. J Biol Chem 282, 28328–28334 (2007). [PubMed: 17631492]

39. Li Y, Park JS, Deng JH & Bai Y Cytochrome c oxidase subunit IV is essential for assembly and respiratory function of the enzyme complex. J Bioenerg Biomembr 38, 283–291 (2006). [PubMed: 17091399]
40. Laganiere J, et al. A polymorphic autoregulatory hormone response element in the human estrogen-related receptor alpha (ERRalpha) promoter dictates peroxisome proliferator-activated receptor gamma coactivator-1alpha control of ERRalpha expression. J Biol Chem 279, 18504–18510 (2004). [PubMed: 14978033]
41. Chaveroux C, et al. Molecular and genetic crosstalks between mTOR and ERRalpha are key determinants of rapamycin-induced nonalcoholic fatty liver. Cell Metab 17, 586–598 (2013). [PubMed: 23562079]
42. Thomas-Chollier M, et al. Transcription factor binding predictions using TRAP for the analysis of ChIP-seq data and regulatory SNPs. Nat Protoc 6, 1860–1869 (2011). [PubMed: 22051799]
43. Kim DK, et al. Orphan nuclear receptor estrogen-related receptor gamma (ERRgamma) is key regulator of hepatic gluconeogenesis. J Biol Chem 287, 21628–21639 (2012). [PubMed: 22549789]
44. Kraus RJ, Ariazi EA, Farrell ML & Mertz JE Estrogen-related receptor alpha 1 actively antagonizes estrogen receptor-regulated transcription in MCF-7 mammary cells. J Biol Chem 277, 24826–24834 (2002). [PubMed: 11986328]
45. Heckler MM, Thakor H, Schafer CC & Riggins RB ERK/MAPK regulates ERRgamma expression, transcriptional activity and receptor-mediated tamoxifen resistance in ER+ breast cancer. FEBS J 281, 2431–2442 (2014). [PubMed: 24684682]
46. Bennett EP, et al. INDEL detection, the 'Achilles heel' of precise genome editing: a survey of methods for accurate profiling of gene editing induced indels. Nucleic Acids Res 48, 11958–11981 (2020). [PubMed: 33170255]
47. Sahu A, et al. Discovery of Targets for Immune-Metabolic Antitumor Drugs Identifies Estrogen-Related Receptor Alpha. Cancer Discov 13, 672–701 (2023). [PubMed: 36745048]
48. Kuleshov MV, et al. Enrichr: a comprehensive gene set enrichment analysis web server 2016 update. Nucleic Acids Res 44, W90–97 (2016). [PubMed: 27141961]
49. Xia H, Dufour CR & Giguere V ERRalpha as a Bridge Between Transcription and Function: Role in Liver Metabolism and Disease. Front Endocrinol (Lausanne) 10, 206 (2019). [PubMed: 31024446]
50. Zielke A, et al. Establishment of a highly differentiated thyroid cancer cell line of Hurthle cell origin. Thyroid 8, 475–483 (1998). [PubMed: 9669284]
51. Mirebeau-Prunier D, et al. Estrogen-related receptor alpha modulates lactate dehydrogenase activity in thyroid tumors. PLoS One 8, e58683 (2013). [PubMed: 23516535]
52. Patch RJ, et al. Identification of diaryl ether-based ligands for estrogen-related receptor alpha as potential antidiabetic agents. J Med Chem 54, 788–808 (2011). [PubMed: 21218783]
53. Nilsson M & Fagman H Development of the thyroid gland. Development 144, 2123–2140 (2017). [PubMed: 28634271]
54. Wojakowska A, et al. Detection of metabolites discriminating subtypes of thyroid cancer: Molecular profiling of FFPE samples using the GC/MS approach. Mol Cell Endocrinol 417, 149–157 (2015). [PubMed: 26415588]
55. Nahm JH, Kim HM & Koo JS Glycolysis-related protein expression in thyroid cancer. Tumour Biol 39, 1010428317695922 (2017). [PubMed: 28347233]
56. Takacova M, et al. Expression pattern of carbonic anhydrase IX in Medullary thyroid carcinoma supports a role for RET-mediated activation of the HIF pathway. Am J Pathol 184, 953–965 (2014). [PubMed: 24518567]
57. Lopez-Penabad L, et al. Prognostic factors in patients with Hurthle cell neoplasms of the thyroid. Cancer 97, 1186–1194 (2003). [PubMed: 12599224]
58. McFadden DG & Sadow PM Genetics, Diagnosis, and Management of Hurthle Cell Thyroid Neoplasms. Front Endocrinol (Lausanne) 12, 696386 (2021). [PubMed: 34177816]

59. Bonora E, et al. Defective oxidative phosphorylation in thyroid oncocytic carcinoma is associated with pathogenic mitochondrial DNA mutations affecting complexes I and III. Cancer Res 66, 6087–6096 (2006). [PubMed: 16778181]
60. Gasparre G, et al. An inherited mitochondrial DNA disruptive mutation shifts to homoplasmy in oncocytic tumor cells. Hum Mutat 30, 391–396 (2009). [PubMed: 19086058]
61. Baris O, et al. Transcriptional profiling reveals coordinated up-regulation of oxidative metabolism genes in thyroid oncocytic tumors. J Clin Endocrinol Metab 89, 994–1005 (2004). [PubMed: 14764826]
62. Savagner F, et al. PGC-1-related coactivator and targets are upregulated in thyroid oncocytoma. Biochem Biophys Res Commun 310, 779–784 (2003). [PubMed: 14550271]
63. Gopal RK, et al. Effectors Enabling Adaptation to Mitochondrial Complex I Loss in Hurthle Cell Carcinoma. Cancer Discov 13, 1904–1921 (2023). [PubMed: 37262067]
64. Frank AR, et al. Mitochondrial-Encoded Complex I Impairment Induces a Targetable Dependency on Aerobic Fermentation in Hurthle Cell Carcinoma of the Thyroid. Cancer Discov 13, 1884–1903 (2023). [PubMed: 37262072]
65. Odate T, et al. Progression of Papillary Thyroid Carcinoma to Anaplastic Carcinoma in Metastatic Lymph Nodes: Solid/Insular Growth and Hobnail Cell Change in Lymph Nodes Are Predictors of Subsequent Anaplastic Transformation. Endocr Pathol 32, 347–356 (2021). [PubMed: 33761111]
66. Ariazi EA, Kraus RJ, Farrell ML, Jordan VC & Mertz JE Estrogen-related receptor alpha1 transcriptional activities are regulated in part via the ErbB2/HER2 signaling pathway. Mol Cancer Res 5, 71–85 (2007). [PubMed: 17259347]
67. Deblois G, St-Pierre J & Giguere V The PGC-1/ERR signaling axis in cancer. Oncogene 32, 3483–3490 (2013). [PubMed: 23208510]
68. Dobin A, et al. STAR: ultrafast universal RNA-seq aligner. Bioinformatics 29, 15–21 (2013). [PubMed: 23104886]
69. Engstrom PG, et al. Systematic evaluation of spliced alignment programs for RNA-seq data. Nat Methods 10, 1185–1191 (2013). [PubMed: 24185836]
70. Bolger AM, Lohse M & Usadel B Trimmomatic: a flexible trimmer for Illumina sequence data. Bioinformatics 30, 2114–2120 (2014). [PubMed: 24695404]
71. Li B & Dewey CN RSEM: accurate transcript quantification from RNA-Seq data with or without a reference genome. BMC Bioinformatics 12, 323 (2011). [PubMed: 21816040]
72. Gu Z, Eils R & Schlesner M Complex heatmaps reveal patterns and correlations in multidimensional genomic data. Bioinformatics 32, 2847–2849 (2016). [PubMed: 27207943]
73. Breiman L Random Forests. Machine Learning 45, 5–32 (2001).
74. Song YS, et al. Aberrant Thyroid-Stimulating Hormone Receptor Signaling Increases VEGF-A and CXCL8 Secretion of Thyroid Cancer Cells, Contributing to Angiogenesis and Tumor Growth. Clin Cancer Res 25, 414–425 (2019). [PubMed: 30314969]
75. Wu PK, et al. A mortalin/HSPA9-mediated switch in tumor-suppressive signaling of Raf/MEK/extracellular signal-regulated kinase. Mol Cell Biol 33, 4051–4067 (2013). [PubMed: 23959801]
76. Ichida M, Nemoto S & Finkel T Identification of a specific molecular repressor of the peroxisome proliferator-activated receptor gamma Coactivator-1 alpha (PGC-1alpha). J Biol Chem 277, 50991–50995 (2002). [PubMed: 12397057]
77. Zhang Y, et al. BAP1 links metabolic regulation of ferroptosis to tumour suppression. Nat Cell Biol 20, 1181–1192 (2018). [PubMed: 30202049]
78. Sanjana NE, Shalem O & Zhang F Improved vectors and genome-wide libraries for CRISPR screening. Nat Methods 11, 783–784 (2014). [PubMed: 25075903]
79. Hong SK, Yoon S, Moelling C, Arthan D & Park JI Noncatalytic function of ERK1/2 can promote Raf/MEK/ERK-mediated growth arrest signaling. J Biol Chem 284, 33006–33018 (2009). [PubMed: 19805545]
80. Karkhanis M & Park JI Sp1 regulates Raf/MEK/ERK-induced p21(CIP1) transcription in TP53-mutated cancer cells. Cell Signal 27, 479–486 (2015). [PubMed: 25595558]

81. Parker JB, Palchaudhuri S, Yin H, Wei J & Chakravarti D A transcriptional regulatory role of the THAP11-HCF-1 complex in colon cancer cell function. Mol Cell Biol 32, 1654–1670 (2012). [PubMed: 22371484]

82. Tariq M, et al. Erasure of CpG methylation in Arabidopsis alters patterns of histone H3 methylation in heterochromatin. Proc Natl Acad Sci U S A 100, 8823–8827 (2003). [PubMed: 12853574]

83. proteinatlas.org, H.P.A.

84. Fisher FMa.R.A. Questions and Answers. The American Statistician 2, 30–31 (1948).

85. Madeira F, et al. The EMBL-EBI search and sequence analysis tools APIs in 2019. Nucleic Acids Res 47, W636–W641 (2019). [PubMed: 30976793]

86. Waterhouse AM, Procter JB, Martin DM, Clamp M & Barton GJ Jalview Version 2--a multiple sequence alignment editor and analysis workbench. Bioinformatics 25, 1189–1191 (2009). [PubMed: 19151095]

87. Fornes O, et al. JASPAR 2020: update of the open-access database of transcription factor binding profiles. Nucleic Acids Res 48, D87–D92 (2020). [PubMed: 31701148]

Statement of significance

This study identifies ESRRA as a tumor type-specific regulator of mortalin expression and demonstrates that the ESRRA-mortalin axis has potential as a biomarker and candidate therapeutic target for thyroid cancer.

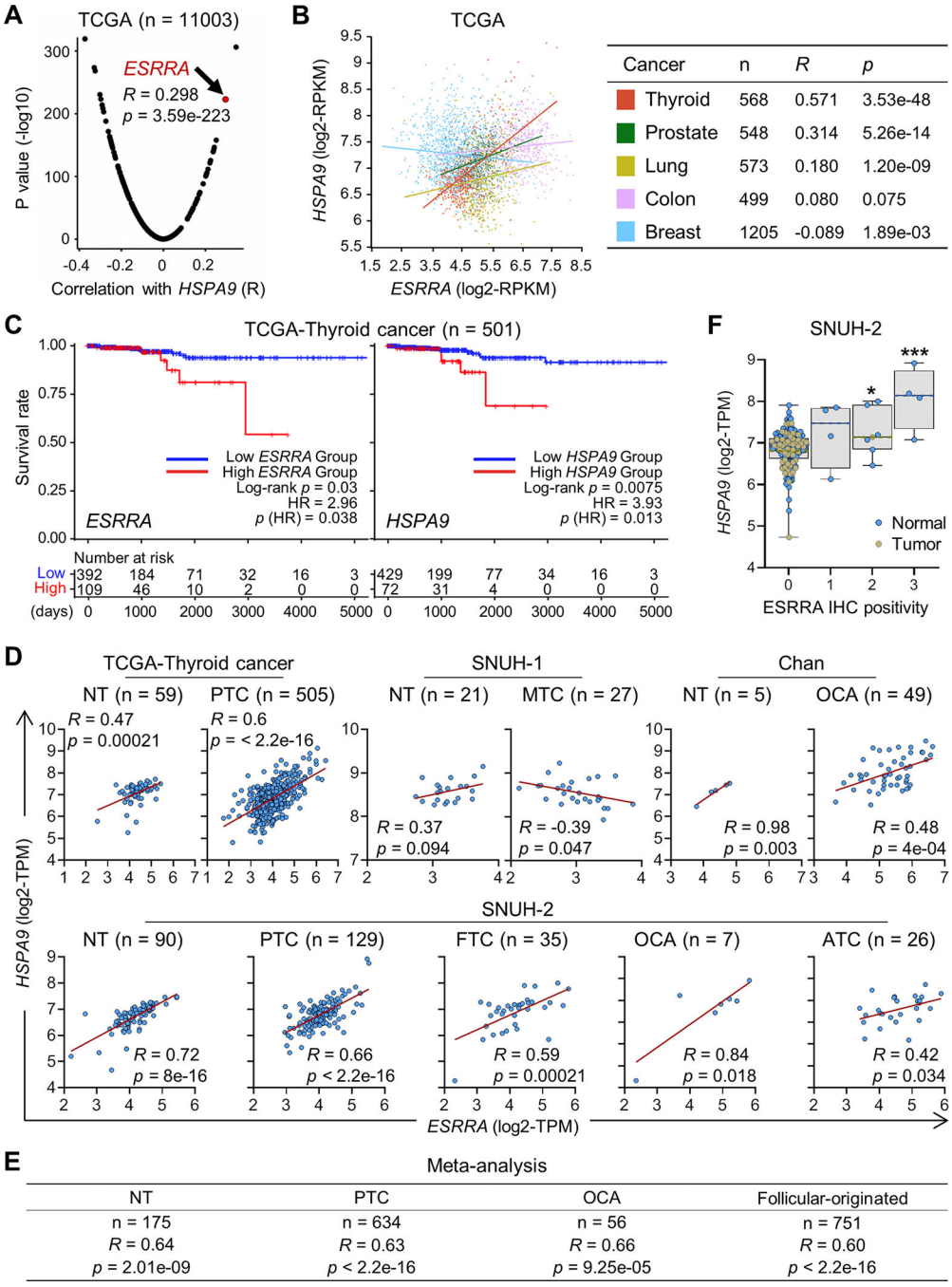

Figure 1. Correlation analysis of *ESRRA* and *HSPA9* in different thyroid tumor subtypes.

(A) Transcription factors expressed in correlation with *HSPA9* in the TCGA datasets available from R2 platform (R2 ID: ps_avgpres_tcgapangdca11003_tcgagdcrs). Volcano plot was generated using R2 [12] to indicate the Pearson's correlation coefficient (*R*) and the significance of association (*p*) of the transcription factors. *R* and *p* values were generated by R2. **(B)** Correlation between *ESRRA* and *HSPA9* RNA levels analyzed for selected tumors in the data in (A). **(C)** Kaplan-Meier plots generated using TCGA-thyroid carcinoma dataset from the Human Protein Atlas using the best cutoff threshold. The number of

events per each timepoint are indicated beneath the plots. *p* values were determined by the Log-rank test. **(D)** Correlation between *ESRRA* and *HSPA9* RNA levels analyzed using the TGCA-thyroid carcinoma [505 PTCs with 59 matched normal thyroid tissues (NTs)], the SNUH RNA-seq datasets (SNUH-1 includes 21 NTs, 27 MTCs; SNUH-2 129 PTCs, 35 FTCs, 7 OCAs and 26 ATCs, and 90 paired NTs), and the Chan group dataset (5 NTs and 49 OCAs). **(E)** Meta-analyses of (D) NT (TCGA, SNUH-1, SNUH-2 and Chan group data), PTC (TCGA and SNUH-2), OCA (SNUH-1 and Chan group data), and follicular-originated tumors combined (TCGA, SNUH-2, and Chan group data). Indicated are aggregated *p* values. **(F)** Distribution of *HSPA9* RNA levels by ESRRA IHC positivity in the SNUH-2 patient cohort. The values in the Box plot range from 25^{th} to 75^{th}. Whiskers indicate minimum to maximum values. Dashed lines indicate the median value of all data-points. $*p < 0.05$, $***p < 0.001$, one-tailed Mann-whitney U test compared to negative ESRRA expression samples.

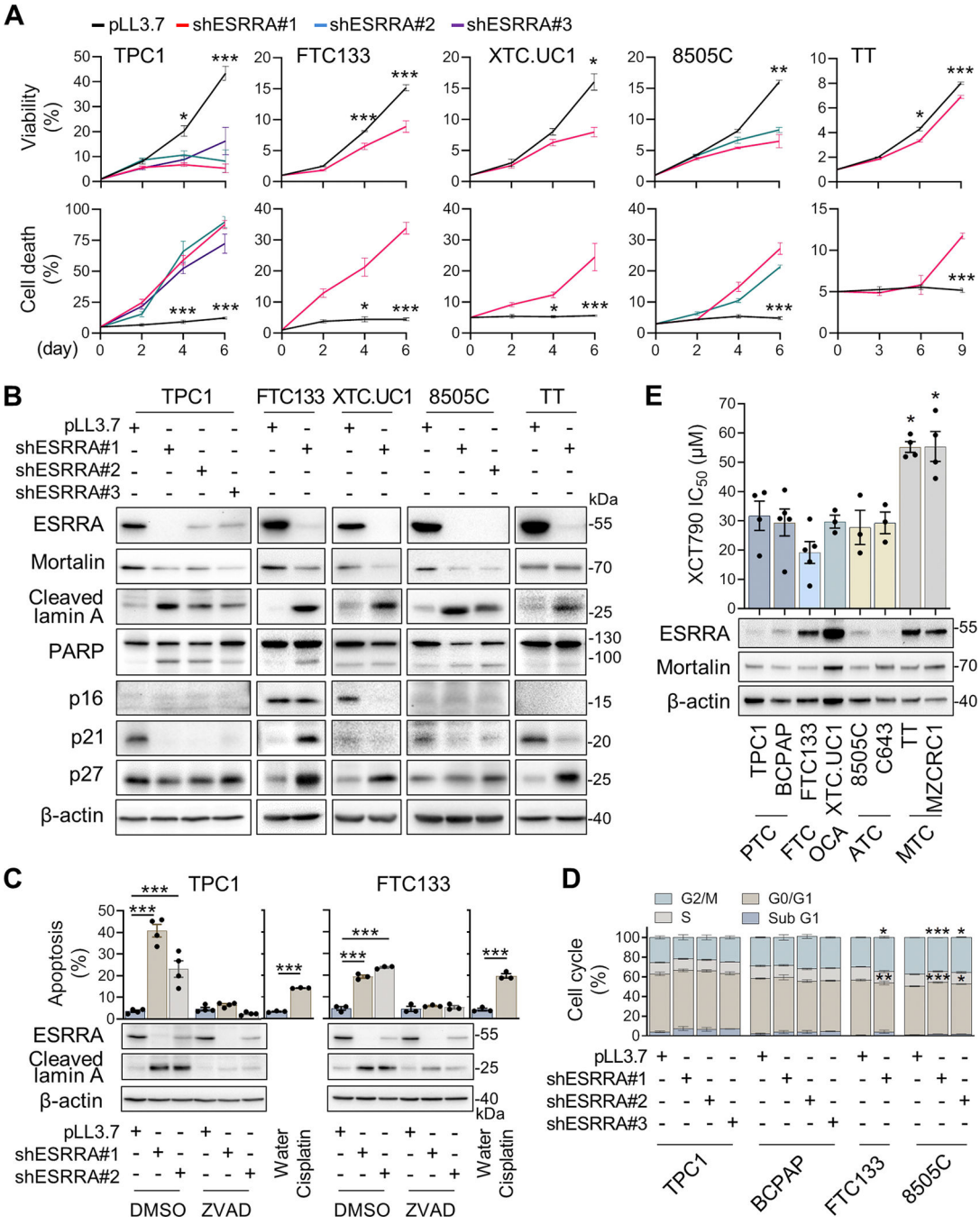

Figure 2. ESRRA depletion suppresses thyroid tumor cell viability through caspase-dependent apoptosis.

(A) Time course cell viability determined by TO-PRO-3 assays (mean ± SEM, n ≥ 3) of cells infected with pLL3.7 lentiviruses expressing different shRNA constructs targeting ESRRA (shESRRA) at the indicated days. $^{**}p < 0.005$, $^{***}p < 0.001$, two-way ANOVA with Bonferroni post-tests. **(B)** Western blotting of total lysates of cells infected with pLL3.7 or shESRRA for 72 h. β-actin is the control for equal protein loading. **(C)** Apoptotic cell death determined by annexin V assays of cells infected with pLL3.7-shESRRA for 72 h with

or without 25 μM ZVAD for 24 h. Western blots are representative images. *$p < 0.05$, ***$p < 0.001$, one-way ANOVA with Bonferroni post-tests. **(D)** Cell cycle analysis determined by propidium iodide staining of cells infected with pLL3.7-shESRRA for 72 h. *$p < 0.05$, **$p < 0.005$, ***$p < 0.001$, two-way ANOVA with Bonferroni post-tests. **(E)** Analysis of IC_{50} values (mean ± SEM, n ≥ 3) determined by crystal violet staining of cells treated with XCT790 for 48 h. *$p < 0.05$, one-way ANOVA with Bonferroni post-tests. ESRRA and mortalin levels of corresponding cell lines were determined by of western blotting.

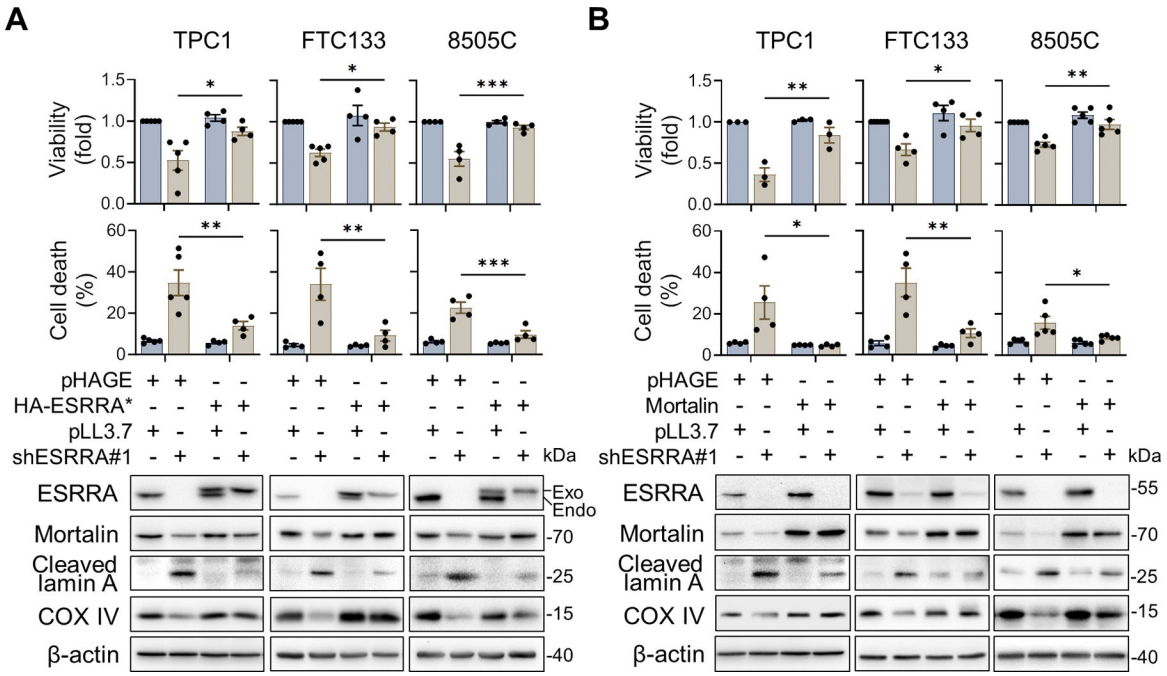

Figure 3. shRNA non-targetable ESRRA and mortalin overexpression rescues ESRRA-depleted cells.

TO-PRO-3 assay of cells infected with pLL3.7-shESRRA#1 virus for 48 h after 48 h overexpression of **(A)** lentiviral pHAGE with N-terminal HA-tagged shRNA non-targetable ESRRA (HA-ESRRA*) and **(B)** lentiviral pHAGE mortalin. Total lysates of these cells were analyzed by western blotting, β-actin is the control for equal protein loading. Data are mean ± SEM, n ≥ 3, *$p < 0.05$, **$p < 0.005$, ***$p < 0.001$, two-way ANOVA with Bonferroni post-tests.

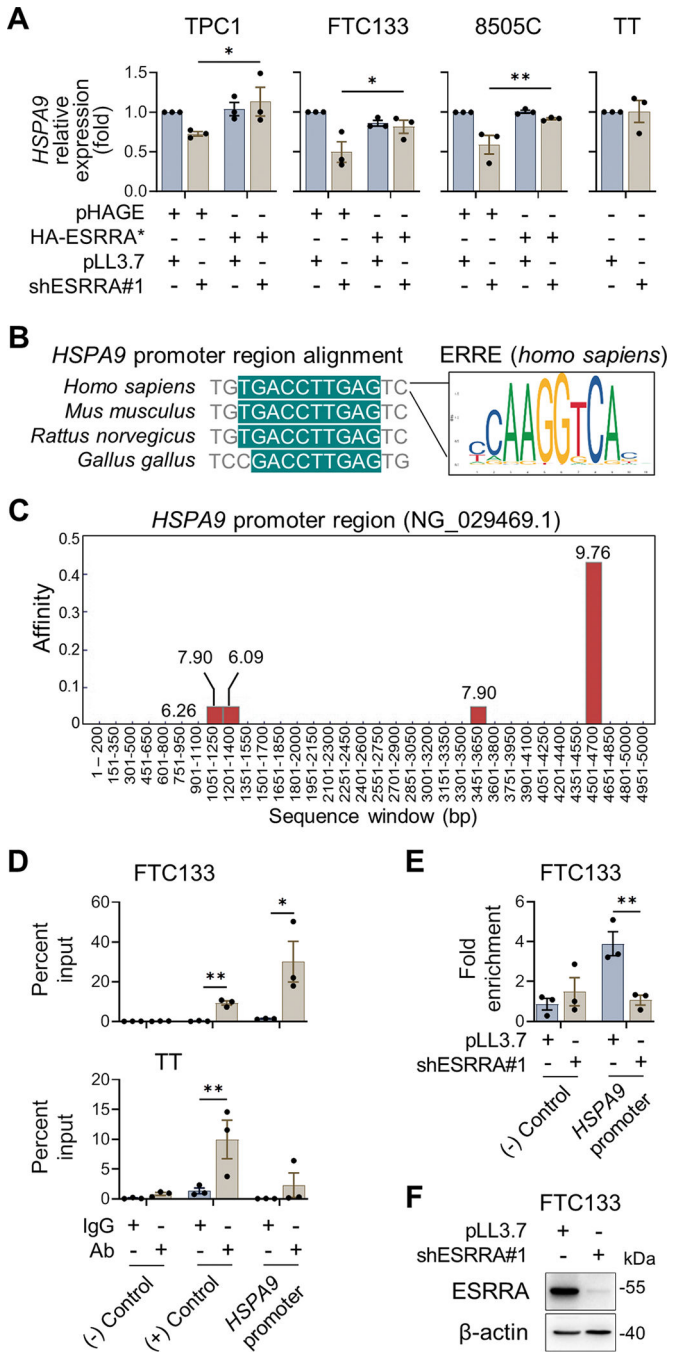

Figure 4. ESRRA increases *HSPA9* expression through an interaction with *HSPA9* promoter in follicular cell-originated tumor cells.

(A) qPCR quantitation of *HSPA9* mRNA levels in cells infected with pLL3.7-shESRRA#1 virus for 48 h after 48 h overexpression of pHAGE-HA-ESRRA* viruses. Data (mean ± SEM, n = 3) were normalized for *ACBT* mRNA levels in the cells. *$p < 0.05$, **$p < 0.005$, two-way ANOVA with Bonferroni post-tests. Two-sample t-test for TT. **(B)** The partial *HSPA9* promoter region of humans, mice, rats, and chickens aligned by Clustal Omega [85] and visualized by Jalview [86]. Highlighted area (teal) indicates predicted ERRE. *Homo*

sapiens ERRE at right is visualized by JASPAR [87]. **(C)** ESRRA binding sites prediction by TRAP [42] using *HSPA9* gene sequence (GenBank NG_029469.1). The bars indicate predicted binding affinities and values indicate weight score. **(D)** ChIP-qPCR analysis (mean ± SEM, n = 3). *$p < 0.05$, two-sample t-test. The ESRRA interaction control oligomers are described in the Method section. **(E)** ChIP-qPCR analysis (mean ± SEM, n = 3) of cells infected with pLL3.7-shESRRA virus for 48 h. **$p < 0.005$, two-sample t-test. **(F)** Western blotting of total lysates of cells in (E).

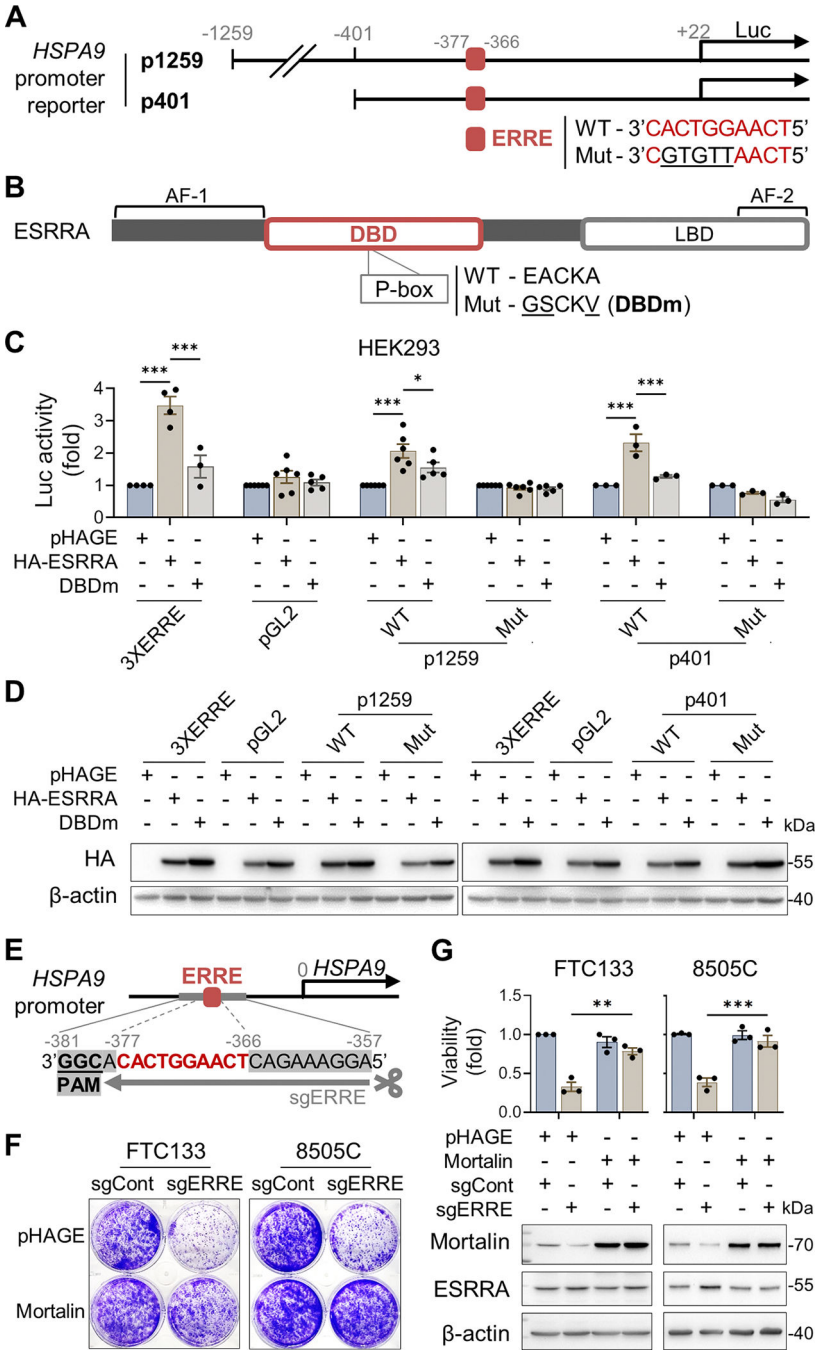

Figure 5. ESRRA increases the activity of *HSPA9* promoter through an ERRE.

(A) Illustration of p1259 and p401 *HSPA9* promoter luciferase reporters. The reporters contain wildtype (WT) or mutant (mut) putative ERRE. **(B)** Illustration of the ESRRA construct and its DNA-binding domain mutant (DBDm). Activation function (AF)-1 and −2 indicate transcriptional activation domains; P-box is proximal-box defines DNA sequence specificity. **(C)** Activity of the luciferase reporters (mean ± SEM, n ≥ 3) in HEK293 cells infected with pHAGE virus expressing HA-ESRRA or HA-ESRRA DBDm for 48 h. *$p < 0.05$, ***$p < 0.001$, two-way ANOVA with Bonferroni post-tests. **(D)** Western blotting

of the assay samples in (C). Shown are representative images. **(E)** Design of CRISPR/Cas9 sgRNA targeting the putative ERRE in *HSPA9* promoter (sgERRE). **(F)** Crystal violet staining of cells infected with the lentiviral sgERRE or its scramble sgRNA control (sgCont). Cells were selected for 2 days with 2 μg/ml puromycin prior to pHAGE-mortalin infection for 5 days. **(G)** Cell viability determined by TO-PRO-3 assays (mean ± SEM, n =3) and Western blotting of total lysates of cells treated as described in (F). $^{**}p < 0.005$, $^{***}p < 0.001$, two-way ANOVA with Bonferroni post-tests.

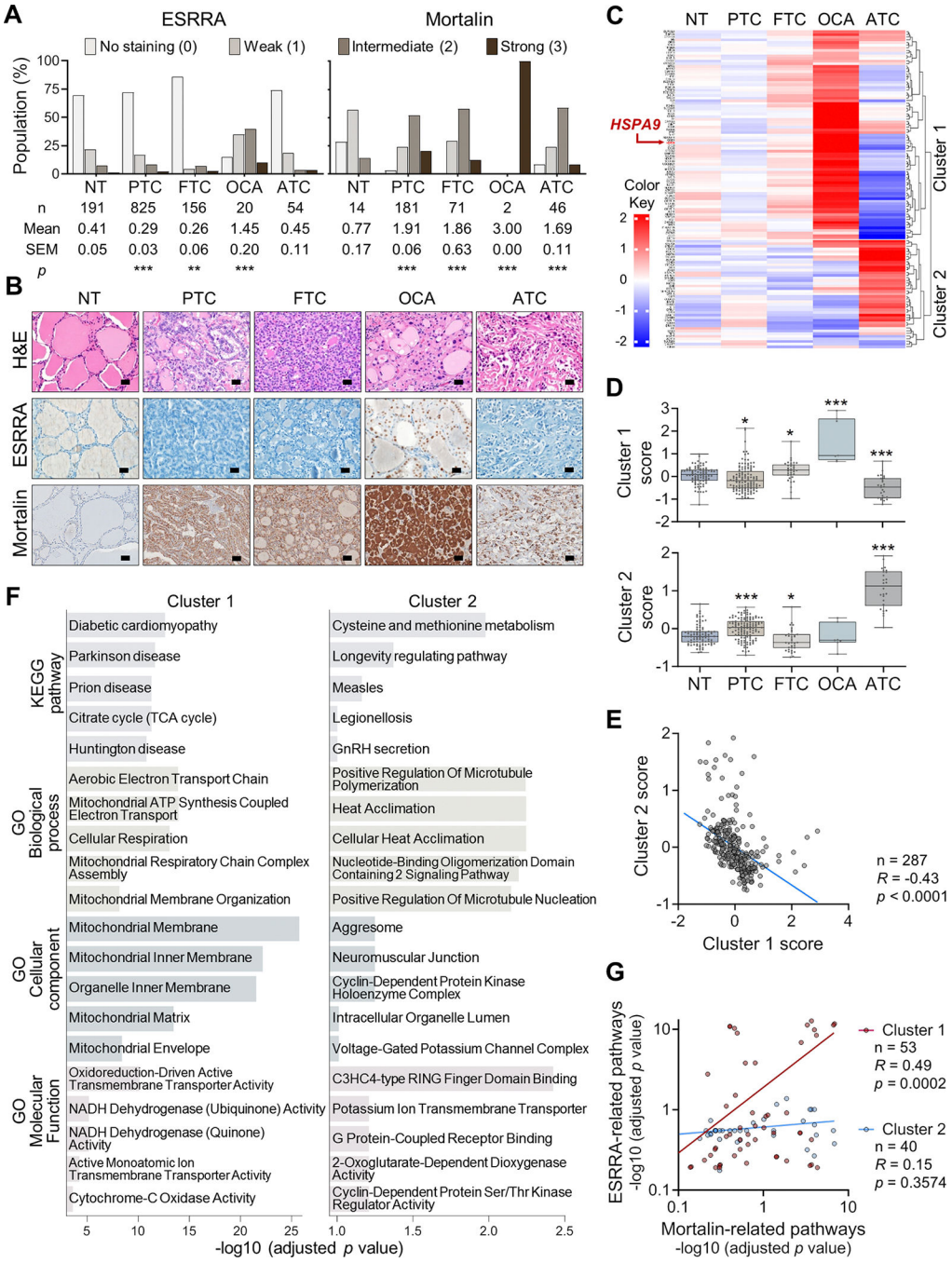

Figure 6. ESRRA expression and activity in different thyroid tumor subtypes.

(A) ESRRA and mortalin protein levels determined by IHC (191 normal thyroids, 825 PTCs, 156 FTCs, 20 OCAs, and 54 ATCs for ESRRA, and 14 thyroids, 181 PTCs, 71 FTCs, 2 OCAs, and 46 ATCs for mortalin). Data are presented as percentage (%) of total population with different IHC staining intensity (0 to 3). $^{**}p < 0.005$, $^{***}p < 0.001$, Kruskal–Wallis test (nonparametric ANOVA) with Dunn post-test for multiple comparison. **(B)** Representative IHC images for (A). Scale bar represents 20 μm. **(C)** A heatmap displaying averaged expression of ESRRA target genes in different thyroid histology in the SNUH-2 RNA-seq

data. The heatmap for individual patient is shown in Fig. S7. Gene expression is represented as variance stabilized (vst) values calculated by R package DESeq2. **(D)** ESRRA Cluster 1 and Cluster 2 scores determined hierarchical clustering. The values in the box plot range from 25^{th} to 75^{th}. Whiskers indicate minimum to maximum values. Lines indicate the median value of all data-points. *$p < 0.05$, ***$p < 0.001$, two-sample t-test. **(E)** Pearson's correlation between ESRRA Cluster 1 and Cluster 2 gene expression determined using the SNUH-2 RNA-seq data. **(F)** Top 5 terms of KEGG and GO enrichment of ESRRA Cluster 1 and Cluster 2 genes. **(G)** Overlap between the mortalin-related pathways and the ESRRA Cluster 1- or Cluster 2-related pathways. Pearson's correlation was calculated based on adjusted p values in −log10 scale.

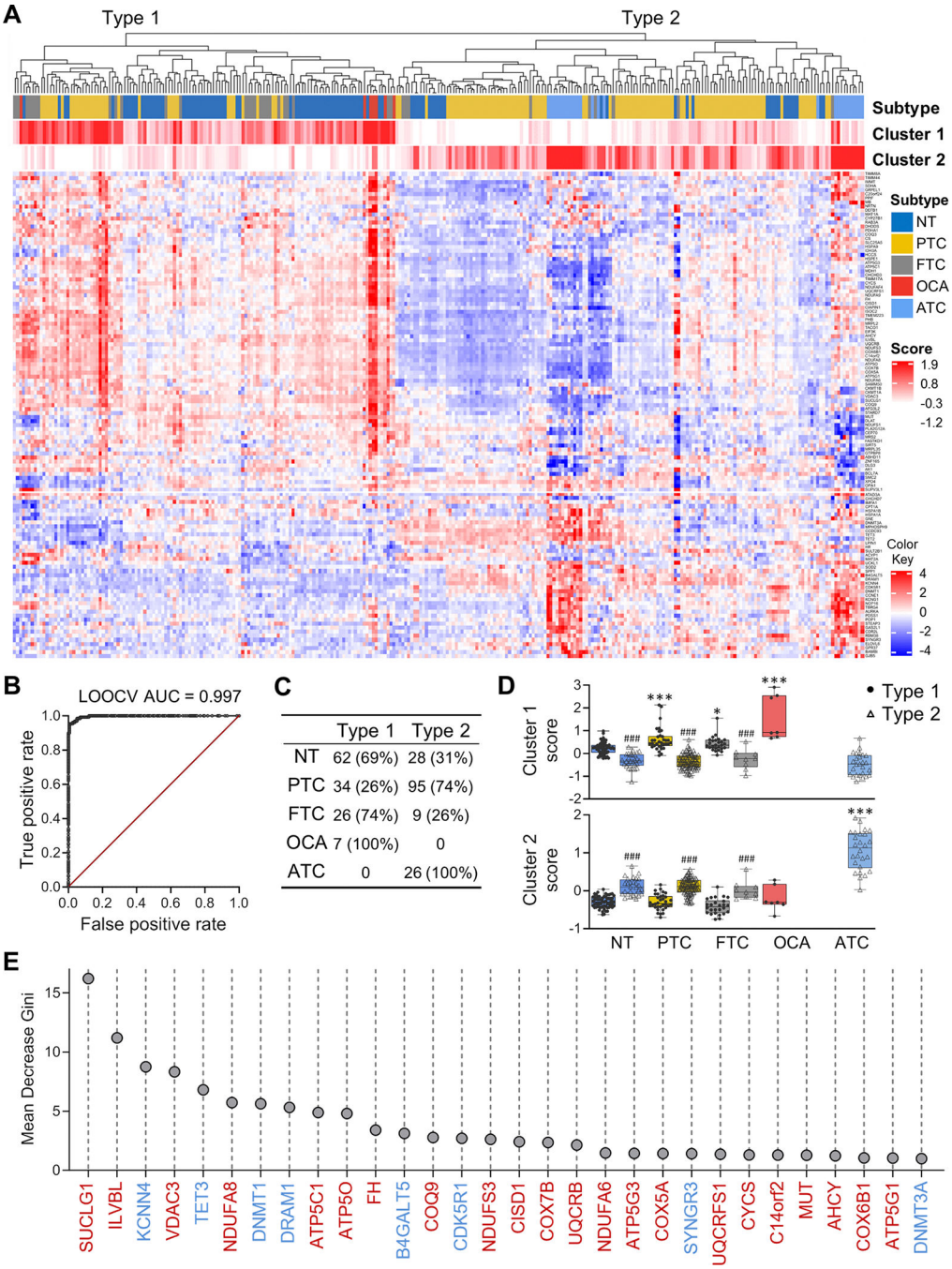

Figure 7. A molecular subtyping using ESRRA signature genes.

(A) A heatmap clustering patient samples for the SNUH-2 RNA-seq data into Type 1 and Type 2 molecular subtypes based on ESRRA target gene expression patterns. **(B)** Receiver operating characteristic (ROC) curve with leave-one-out cross validation (LOOCV) generated from random forest algorithm for Type 1 and Type 2 classification and with the value of area under curve (AUC) calculated. **(C)** Histology-based distribution of Type 1 and Type 2 samples in (A). **(D)** Cluster 1 and Cluster 2 scores of Type1 and Type 2 samples by subtypes. The values in the box plot range from 25th to 75th. Whiskers indicate minimum

to maximum values. Lines indicate the median value of all data-points. *$p < 0.05$, ***$p < 0.001$, two-sample t-test of Type 1 or Type 2 tumor subtypes compared to the same type of normal thyroid samples. $^{\#\#\#}p < 0.001$, two-sample t-test of different types within the same subtypes. **(E)** Top 30 ESRRA target genes predicted by the random forest algorithm to have larger influence on Type 1 and Type 2 classification. Red and blue indicate the genes in Cluster 1 and Cluster 2, respectively.

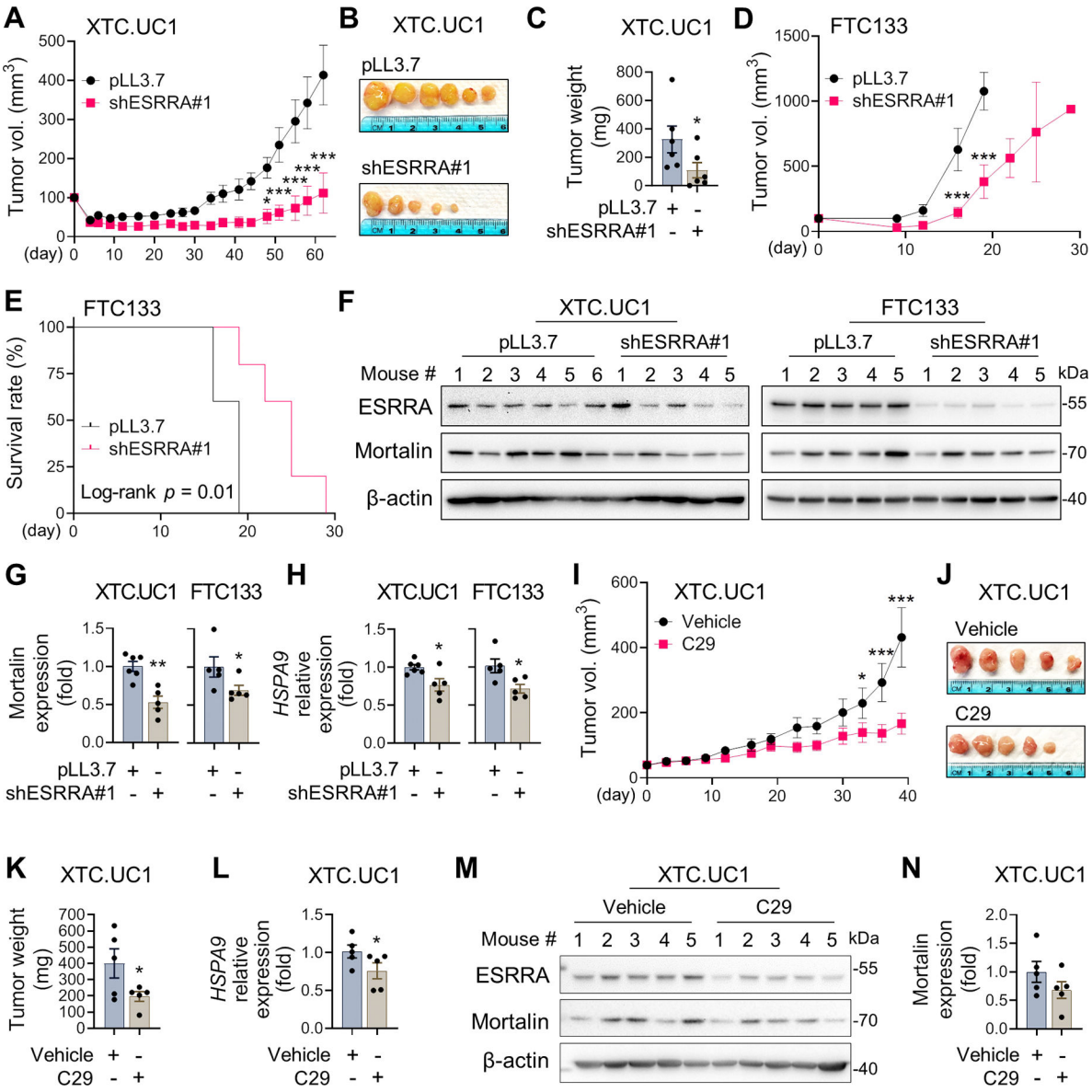

Figure 8. ESRRA knockdown suppresses the growth of XTC.UC1 and FTC133 xenografts in athymic nude mice.

(A) Changes in tumor volume (mean ± SEM, n = 6) of XTC.UC1 xenografts infected with pLL3.7-shESRRA#1 and the control virus. $p < 0.001$ (pLL3.7 vs. shESRRA#1, mixed effects model analysis). *$p < 0.05$, ***$p < 0.001$ (adjusted for multiple comparisons by Bonferroni tests, interaction terms included). **(B)** Images of XTC.UC1 tumors harvested at the end of the experiment. One of the ESRRA-knocked down tumors was too small to collect. **(C)** Weight (mean ± SEM, n = 6 for control, n = 6 for shESRRA) of tumors in (B). *$p < 0.05$, two-sample t-test. **(D)** Changes in tumor volume (mean ± SEM, n = 5) of FTC133 xenografts infected with pLL3.7-shESRRA#1 and the control virus. $p = 0.001$ (pLL3.7 vs. shESRRA#1, mixed effects model analysis). ***$p < 0.001$ (adjusted for multiple comparisons by Bonferroni tests, interaction terms included). **(E)** Probability of animal survival in (B) determined by Kaplan-Meier curves. p values were determined by

the Log-rank test. Mice were sacrificed when tumor size reached 1000 mm^3. **(F)** Western blotting of homogenates of the tumors harvested in (B) and (E). **(G)** Densitometry of mortalin signals in the Western blots in (F) normalized by β-actin signals. *$p < 0.05$, **$p < 0.005$, two-sample t-test. **(H)** qPCR quantitation of *HSPA9* mRNA levels in the tumors harvested in (B) and (E). *ACBT* mRNA levels were used for normalization. *$p < 0.05$, two-sample t-test. **(I)** Changes in tumor volume (mean ± SEM, n = 5) of XTC.UC1 xenografts treated with C29 and the control vehicle. $p = 0.03$ (vehicle vs. C29, mixed effects model analysis). *$p < 0.05$, ***$p < 0.001$ (adjusted for multiple comparisons by Bonferroni tests, interaction terms included). **(J)** Images of tumors harvested at the end of the experiment in (I). **(K)** Weights (mean ± SEM, n = 5) of tumors in (J). *$p < 0.05$, two-sample t-test. **(L)** qPCR quantitation of *HSPA9* mRNA levels in the tumors harvested in (J). *ACBT* mRNA levels were used for normalization. *$p < 0.05$, two-sample t-test. **(M)** Western blotting of tumor homogenates harvested in (J). **(N)** Densitometry of mortalin signals in the Western blots in (M) normalized by β-actin signals.